Physics – Uspekhi **57** (2) 105 – 127 (2014)

REVIEWS OF TOPICAL PROBLEMS PACS numbers: **71.30.+h**, 73.40.Qv, **73.43.–f**

Integer quantum Hall effect and related phenomena

V T Dolgopolov

DOI: 10.3367/UFNe.0184.201402a.0113

Contents

Abstract. Experimental and theoretical research on the integer quantum Hall effect is reviewed, together with other transport phenomena in a two-dimensional electron gas in a quantizing magnetic field. Particular emphasis is placed on primary experimental data, on the comparison of experimental and theoretical results, and on the analysis of theoretical predictions from the point of view of their experimental verification. Among experiments conducted in recent years, those that have raised questions to be resolved are highlighted. Possible directions of further research are suggested.

1. Introduction

The quantum Hall effect (QHE), discovered in 1980 by K von Klitzing [1], still remains a subject for experimental studies and as before stimulates the work of theorists. The history of research on this effect has developed in such a way that, on average, every five years either new theoretical ideas or experimental breakthroughs have been presented. The diminishing interest in the quantum Hall effect gave way again to rising, so there is no reason for this quasiperiodic process to stop.

During the considerable period of time since its discovery, the integer quantum Hall effect not only has become a topic of modern literature reviews (see, for example, Refs [2–6]), but also has been described in textbooks [7–10]. This poses a question: does one need another review on this topical problem?

The present review was motivated by the fact that the scientific literature mostly shows theoretical aspects and not the experimental state of the art. In the case of the quantum Hall effect, this leads to a curious occurrence: the constructed theories are so attractive that even experimentally unverifiable predictions are treated in textbooks as real ones. The author of this review had the goal to first describe, as broadly and explicitly as possible, the primary experimental results, and second, to highlight those theoretical constructions that lead to unobservable predictions.

2. The subject of discovery

The quantum Hall effect was first observed on a silicon field-effect structure, which is described in a large number of books (see, for example, Ref. [11]). At this stage of the discussion, neither details of the device nor the electron spectrum of the semiconductor is important. The only significant fact is that a two-dimensional electron gas (2DEG) resides at the interface between the semiconductor (Si(100)) and the insulator (SiO_2). The term 'two-dimensional' means that the motion of the electrons is free only in the plane, being quantized in the direction perpendicular to the interface, and all electrons occupy the ground quantum level. The electron system is

V T Dolgopolov Institute of Solid State Physics,
Russian Academy of Sciences,
ul. Akademika Osip'yana 2, 142432 Chernogolovka, Moscow region,
Russian Federation
E-mail: dolgop@issp.ac.ru

Received 9 September 2013, revised 11 October 2013
Uspekhi Fizicheskikh Nauk **184** (2) 113 – 136 (2014)
DOI: 10.3367/UFNr.0184.201402a.0113
Translated by A L Chekhov; edited by A Radzig

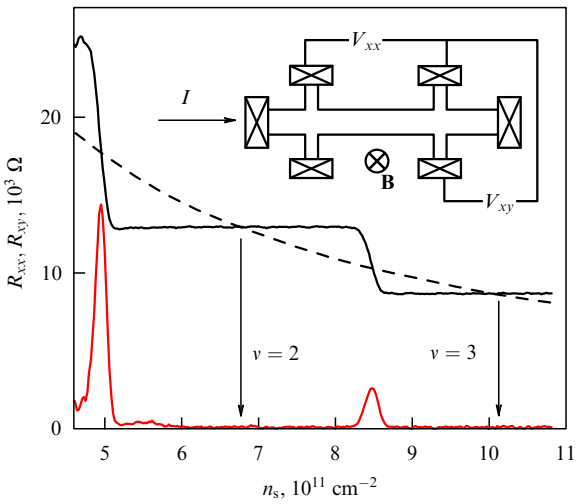

Figure 1. The dependence of the Hall (R_{xy}) and the diagonal (R_{xx}) components of the magnetoresistance tensor on the concentration of a two-dimensional electron gas in a sample based on the silicon field-effect transistor Si-MOSFET(100) (MOSFET: Metal-Oxide-Semiconductor Field-Effect Transistor), at $B = 14$ T, $T = 30$ mK. The sample and the potentials being measured are schematically shown in the inset.

shaped into a Hall bar with ohmic contacts to conduct the measurement current I, and potential contacts to measure voltages V_{xx} and V_{xy} (see inset to Fig. 1). The most important fact is that one can smoothly change the electron concentration in silicon field-effect structures and control it with an accuracy of up to 1%.

Figure 1 shows the experimental results obtained in a silicon field-effect structure similar to the one studied in Ref. [1] but having a higher quality. The experiment was performed at a temperature (30 mK) lower than in Ref. [1]. As seen from the figure, both components $R_{xx} = V_{xx}/I$ and $R_{xy} = V_{xy}/I$ of the magnetoresistance tensor show quite extraordinary behavior in a magnetic field perpendicular to the plane of the two-dimensional electron gas. Indeed, for an ideal sample in a homogeneous electric field E, all electrons drift in the direction perpendicular to the magnetic and electric fields with a speed of cE/B; in such a system, therefore, one should expect that $R_{xx}(n_s) = 0$ and $R_{xy} = B/n_s ec$, where n_s is the electron density, e is the electron charge, and c is the speed of light in a vacuum. The expectant dependence for R_{xy} is plotted in Fig. 1 by a dashed line.

In fact, the Hall component of the resistance tensor shows not a smooth but a stepwise dependence, with wide plateaus and abrupt steps between them. The dissipative component of the magnetoresistance tensor is close to zero on the plateau, but in transition regions it is finite. It was discovered already in the first precise experiments that the resistance at the midpoint of the plateau is given by the relation

$$R_{xy}^{\nu} = \frac{h}{e^2 \nu}, \quad \nu = 1, 2, \ldots, \tag{1}$$

with an accuracy of not less than six significant digits. Moreover, the Hall resistance on the plateau depended neither on the quality or size of the sample nor on the position of the potential contacts.

Thereby, the discovery of the integer quantum Hall effect turned out to be the discovery of a physical representation of a number h/e^2, a combination of universal physical constants. Currently, this combination is known with an accuracy of more than 11 decimal digits, and the value of the Hall resistance on the plateau is adopted as the resistance standard.

Since the appearance of a plateau in the $R_{xy}(n_s)$-dependence is impossible in a pure electron system, one is obliged to relate the observed effect with a chaotic potential in which the electron system dwells. On the other hand, the remarkable accuracy of measurements of universal physical constants in 'dirty' systems is not accidental and has to be linked to some fundamental principle. The search for this principle is one of the main issues in understanding the physical grounds of the integer quantum Hall effect. Another important question is the determination of the physical parameters that limit the accuracy of reproduction of the Hall resistance on the plateaus for different samples. While the first issue was at least partially solved [12], the second one remains unsolved.

3. Ideal electron system in a quantizing magnetic field

3.1 Energy spectrum

The electron gas spectrum in a quantizing magnetic field has been discussed in many textbooks (see, for example, Ref. [13]); therefore, we will restrict ourselves to a short review. It is assumed that the electron gas is situated in the plane (xy), and the magnetic field H is directed along the z-axis. To simplify further discussion, we will introduce a static electric potential depending on a single coordinate $V(x)$. In the Landau gauge, the vector potential has the form $\mathbf{A} = (0, xH, 0)$. In terms of $\mathbf{A}$, we can express the magnetic field $\mathbf{B} = \mathbf{H} = \mathrm{rot}\,\mathbf{A}$ and the kinetic part of the Hamiltonian, $\hat{H} = (\mathbf{p} - (e/c)\,\mathbf{A})^2/2m$, where $\mathbf{p} = -\mathrm{i}\hbar\nabla$, and m is the electron effective mass. This leads to the Schrödinger equation in the form

$$\left[p_x^2 + \left(p_y - x\,\frac{eB}{c}\right)^2 + 2mV(x)\right]\psi(x,y) = 2m\varepsilon\psi(x,y)\,. \tag{2}$$

It is convenient to search for the solution of equation (2) in the form of a plane wave propagating along the y-axis — that is, an exponential $\exp(\mathrm{i}ky)$ multiplied by a function depending only on x. Substituting such a solution into equation (2) yields the one-dimensional Schrödinger equation

$$\left[-\frac{\hbar^2}{2m}\,\frac{\partial^2}{\partial x^2} + \frac{m\omega_c^2}{2}\,(x - x_0)^2 + V(x)\right]\psi(x) = \varepsilon\psi(x)\,, \tag{3}$$

where $\omega_c = eB/mc$ is the cyclotron frequency, $x_0 = kl^2 = k\,c\hbar/(eB)$ is the guiding center coordinate, and l is the magnetic length.

For every value of k, equation (3) corresponds to a discrete set of quantum energy levels. The number of different k values per unit area can be derived in the following way. Let us pick out a rectangle with sides L_x and L_y. The guiding center coordinate falls in the interval $0 < x_0 < L_x$. Consequently, one has $0 < k < L_x/l^2$. At the same time, periodic boundary conditions have to be fulfilled along the y-axis: $k_i = 2\pi i/L_y$, where i is an integer. Hence, $\Delta k = 2\pi/L_y$, and we obtain $n_0 = 1/2\pi l^2$.

Classification of quantum states based on a quasi-continuous set of wave vectors k_y is valid for any one-dimensional

potential $V(x)$. Further, we will discuss the three potentials most important from the experimental viewpoint.

3.2 The case of $V(x)=0$. Quantization condition

As follows from equation (3), at $V(x) = 0$ the electron moves in a parabolic potential well, its energy spectrum being determined by the condition

$$\varepsilon_n = \left(n + \frac{1}{2}\right)\hbar\omega_c\,, \tag{4}$$

while a set of the wave functions is given by a set of harmonic oscillator eigenfunctions. Every energy level splits into two spin sublevels with the energies described in the simplest case by the relation $\pm\mu_B\, gB$, where μ_B is the Bohr magneton, and g is the Landé factor.

The electron density in two-dimensional electron systems is determined, with a high degree of accuracy, by the compensating charge. Therefore, the chemical potential is not fixed but shows sawtooth behavior, as illustrated in Fig. 2. The jumps of the chemical potential occur under the condition $n_s = Nn_0$, where $N = 1, 2, ...$, i.e., for integer filling factor $\nu = N$. Precisely this condition, setting the periodicity in the reciprocal magnetic field $1/B$, determines the period of any quantum oscillations and corresponds approximately to the midpoint of a Hall plateau (see Fig. 1).

3.3 Homogeneous electric field

The electric potential in a homogeneous electric field has the form $V(x) = -eEx$. Adding a linear term to a parabolic potential only shifts its center — that is, x_0 in Eqn (3) is replaced by $x_1 = x_0 + x_E$, where $x_E = eE/(m\omega_c^2)$. The set of quantum energy levels is still described by relation (4), but the whole ladder of energy levels is shifted by a value of $-eE(x_0 + x_E/2)$. This leads to two consequences. First, an ideal electron system can screen long-period potentials, even when the filling factor is an integer: $\nu = N$. The screening turns out to be peculiar: the change in the electron density is determined by the second spatial derivative of the potential. Second, every electron in a homogeneous field acquires a group velocity that is perpendicular to the electric and magnetic field directions:

$$v = \frac{\partial\varepsilon}{\partial k_y} = l^2\,\frac{\partial\varepsilon}{\partial x_0} = \frac{cE}{B}\,, \tag{5}$$

and for an integer filling factor, one finds $\sigma_{xx}=0$, and $\sigma_{xy}=Nn_0ev/E = Ne^2/h$. The Hall resistance changes with the electron concentration monotonically and takes quantized values when the filling factor is an integer, as shown in Fig. 1 by a dashed line.

3.4 Sample bounded by an infinitely high vertical potential barrier

Let us consider now a two-dimensional electron gas that occupies a half-plane $x > 0$, bounded by an infinitely high potential barrier at $x = 0$ (Fig. 3). The effective potential well that is present in Eqn (3) is shown in the inset to Fig. 3. The well is formed by a part of the magnetic parabola cut by a vertical potential wall. The resulting well confines the motion of the electron more strongly than the initial parabola; therefore, the quantum energy levels inside it are higher than the ones determined by relation (4). Moreover, the energy spectrum becomes nonequidistant.

Figure 3 qualitatively illustrates the behavior of the first two lower levels of the energy spectrum as the guiding center changes its position. As the guiding center approaches the vertical barrier, starting from distances comparable to the magnetic length, the energies of both levels increase rapidly compared to the energy in the depth of the two-dimensional electron system. The guiding center, as shown in Fig. 3, can be located outside of the half-plane $x > 0$, but the corresponding electron wave function is limited by the boundaries of this half-plane.

In a spatially bounded ideal two-dimensional electron system, the density of states in every energy gap, although small, is finite due to the upward bending of the quantum levels. As a result, the chemical potential can be fixed at any energy exceeding the lowest quantum level in the bulk of the system (Fig. 3). The dependence of the energy on the guiding center coordinate implies its dependence on k_y, and the fact that an electron has a group velocity v in the y-direction. This means that a nondissipative electric current flows along the

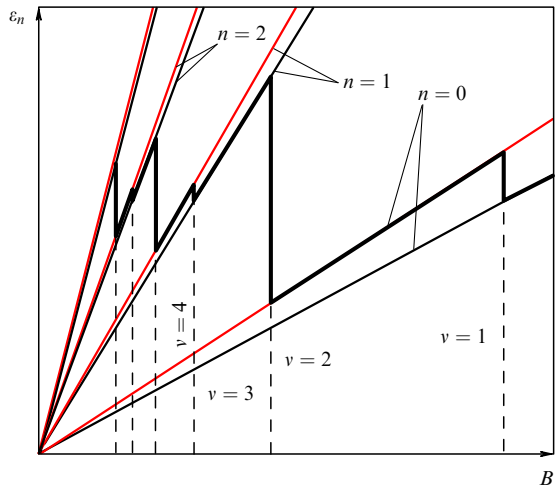

Figure 2. Energy levels (with spin splitting taken into account) of the electron system in a homogeneous quantizing magnetic field. The bold solid line represents the dependence of the system's chemical potential on the magnetic field; $\nu = n_s/n_0$ is the filling factor.

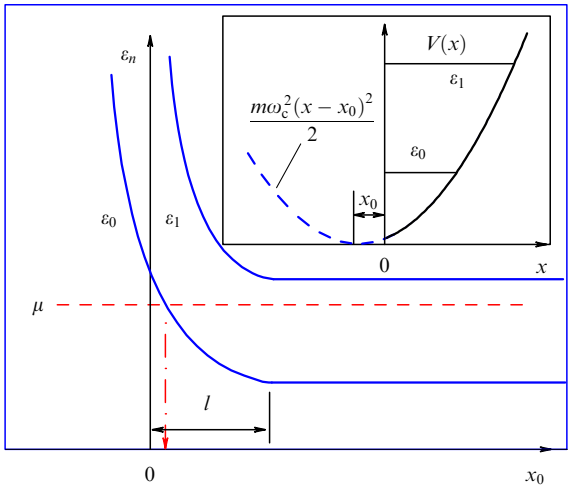

Figure 3. Schematic dependence of the energies ε_0 and ε_1 of the first two lower quantum levels on the coordinate x_0 of the guiding center. The vertical dashed-dotted arrow indicates the position of the edge channel on the abscissa. The effective potential well for the electron is shown in the inset.

edge. Let us calculate its value for the case demonstrated in Fig. 3:

$$I_{\text{left}} = \frac{e}{2\pi}\int_{k_y(\text{left})}^{\infty} v\,\mathrm{d}k_y = \frac{e}{2\pi\hbar}\int_{k_y(\text{left})}^{\infty}\frac{\partial\varepsilon}{\partial k_y}\,\mathrm{d}k_y$$
$$= \frac{e}{h}\int_{\mu}^{\varepsilon_0}\mathrm{d}\varepsilon = \frac{e}{h}\,(\varepsilon_0 - \mu_{\text{left}})\,. \qquad (6)$$

If the electron system has the form of a stripe, a reversed current will flow along its right-hand side. The total current through the cross section of the stripe is given by

$$I = \frac{e}{h}\,(\mu_{\text{right}} - \mu_{\text{left}})\,. \qquad (7)$$

As long as the electron system is in equilibrium, one has $\mu_{\text{right}} = \mu_{\text{left}} = \mu$. The currents flowing along different sides of the sample compensate each other. There remains only the nondissipative diamagnetic current flowing along the edge. In the absence of equilibrium, $\mu_{\text{right}} - \mu_{\text{left}} = eV$, and relation (7) generalized to the case of a few number of quantum energy levels below the level of the chemical potential coincides with relation (1).

The additional charge required to support the chemical potential difference in an ideal sample can be placed only on the edge of the stripe; therefore, the Hall electric field and the resulting Hall current will unavoidably be inhomogeneous [14]. Nevertheless, the total current, according to Eqn (7), does not depend on the field distribution inside the sample, which can be easily derived from Eqn (6) by interpreting ε_0 as the minimal energy of the corresponding quantum energy level in the stripe.

A new opportunity in understanding the integer quantum Hall effect emerges if one considers the nondissipative edge current carried by one or several one-dimensional edge channels, each one carrying the current $I_n = \mu_n e/h$. A detailed consideration, first introduced in Ref. [15], became widespread due to the implementation of the Landauer technique for the integer quantum Hall effect [16] (Fig. 4). Edge channels are visualized for clarity as the intersection lines between the chemical potential level and the bent energy level in the plane assigning the position of the guiding center. Notice explicitly that, in the case of a sufficiently steep wall (vertical, for example), the image of the edge channel defined in such a way can be located outside of the sample.

Another problem regarding the edge channels in an ideal sample was solved experimentally. This problem is connected with the energy dissipation. Indeed, the existence of a current in the presence of a finite chemical potential difference $\Delta\mu$ leads to the power dissipation $(n/h)(\Delta\mu)^2$. Experiments have been performed in Ref. [17] on visualizing the hot spot on the Hall bar in order to find the area where the energy dissipation occurs. It turned out that the dissipation occurs in the corner of the bar (it was shown later that the dissipation is present in two corners on a single diagonal [18]), and the corner changes for a different magnetic field direction (Fig. 5). The choice of the corner depends on the condition that the group velocity of the electrons leaving the electrode be directed along the contact, so that the chemical potentials of the electrons in the edge channel and in the contact coincide along the propagation path of the electrons.

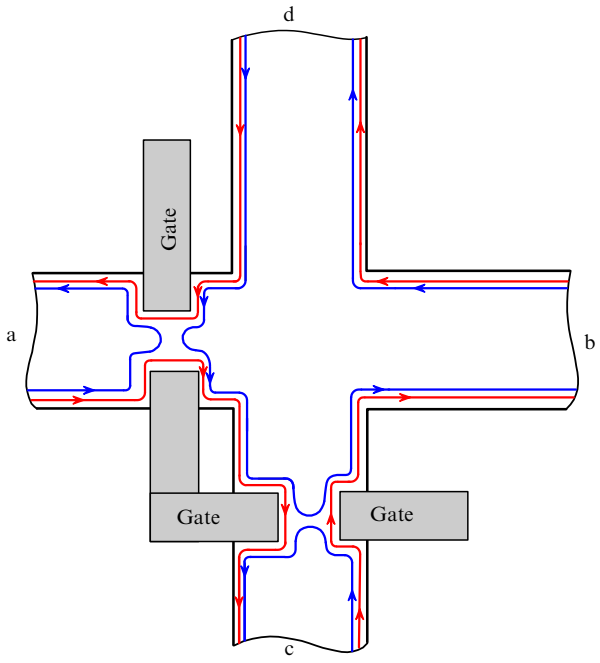

Figure 4. One of the sample's geometries, in which the Landauer–Büttiker formalism is convenient for calculation. Potential contacts a, b, c, d have different chemical potential values. The gate voltages are chosen in such a way that one of the edge channels connects neighboring contacts, and the second one has a controlled transmission coefficient in every narrow area. By setting the transmission coefficients and the chemical potentials of two of the four contacts, one can calculate all the currents and chemical potentials of the other two.

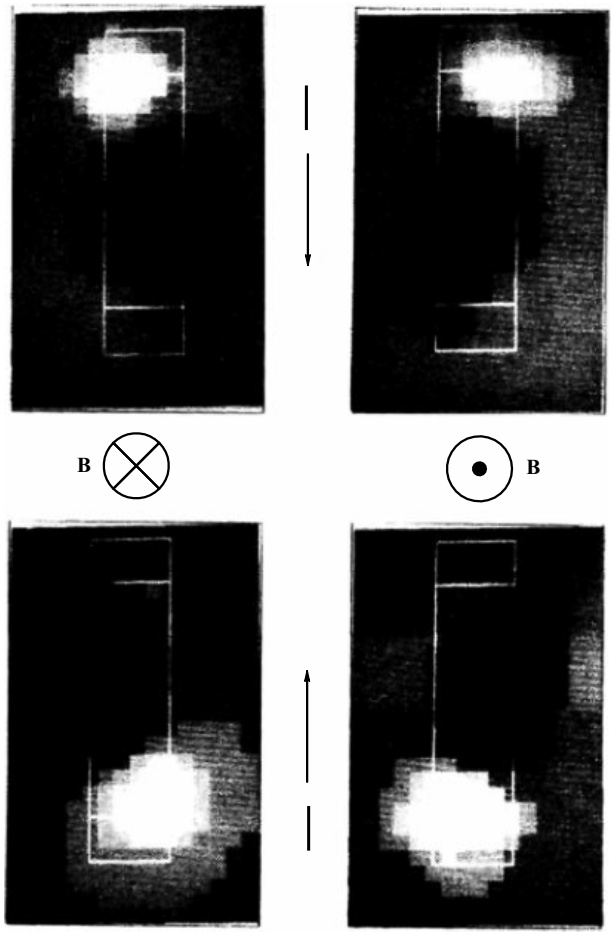

Figure 5. Visualization of the hot spot on the Hall bar under the conditions of the quantum Hall effect. Bright lines mark the boundaries of the two-dimensional electron gas and the electric current contacts. (Data taken from Ref. [17].)

3.5 Compressible and incompressible stripes on an edge of an ideal two-dimensional electron gas

In this section, we will consider an ideal two-dimensional electron gas that is spatially bounded with a smooth potential. The word 'smooth' means that the change of the electron energy on the magnetic length scale is small in comparison to the cyclotron energy. In real semiconductor two-dimensional systems, the potentials often fall into this type.

The terminology used below is not commonly known. Let us explain it. In addition to the usual single-particle density of states $\partial n/\partial\varepsilon$, one can introduce a thermodynamic density of states $\partial n_s/\partial\mu$ proportional to the compressibility of the electron system (see, for example, Ref. [19]). The thermodynamic density of states depends on the temperature and can be nonzero in energy intervals where the single-particle density of states is exactly zero. If the chemical potential, as in Fig. 3, is located between the quantum energy levels, the thermodynamic density of states at zero temperature is close to zero and the electron system is incompressible.

Let us first consider the behavior of the bottom of the electron subband in the absence of a magnetic field (Fig. 6a). In this case, the bottom of the conduction band below the chemical potential level follows the profile of the screened potential. In the case of a parabolic dispersion relation, it also follows the profile of the electron density up to a numerical factor, because in the system under consideration the relationships $\partial n/\partial\varepsilon = \partial n_s/\partial\mu_0 = \text{const}$ are valid.

Let us turn now to the case of a quantizing magnetic field. The coordinate dependence of the profile of the conduction-band bottom cannot remain unchanged in the presence of the quantizing magnetic field [20]. Indeed, the electron density at every quantum energy level remains the same, as long as the quantum level is placed below the chemical potential level. The conservation of the profile of the conduction-band bottom would induce uncompensated electrical charges and fields, which are energetically unfavorable.

Figure 6b depicts the real profile of the conduction-band bottom as a function of the guiding-center coordinate for two Landau levels completely filled in the bulk. As already mentioned, the main condition determining the electron density is the electroneutrality condition. In a quantizing magnetic field, therefore, the electron density dependence on the coordinate should be roughly the same as the one in the absence of the field. The electron density is zero at the intersection point of the band bottom with the chemical potential and starts increasing along the positive direction of the coordinate until it reaches the n_0 value. In the region where the electron density increases, the lowest Landau level is 'pinned' to the chemical potential, because we assume that the density of states in an ideal system has a δ-behavior, i.e., is similar to the behavior of the delta-function. This region is called the compressible liquid. The stripe of the incompressible electron liquid is located to the right of it. The chemical potential crosses there the spectral gap between the Landau levels, and the bottom of the conduction band drops down by $\hbar\omega_c$. The electron concentration is fixed at the density n_0; therefore, the electroneutrality condition is violated. After that, everything repeats: the next Landau level becomes pinned to the chemical potential, and the electron density increases until it reaches the value of $2n_0$, and so forth.

It is easy to estimate the width of the stripe of the incompressible electron liquid. This stripe constitutes a one-dimensional charged object with the excess charge density:

$$e\delta n = e\big(n(x) - n_0\big) = e\,\frac{\partial n}{\partial x}\bigg|_{x=x_0}(x - x_0)\,,$$

where $n(x)$ is the electron concentration in the absence of a magnetic field, and n_0 the fixed electron density within the stripe. The electric field induced in the plane is estimated by $(ea/\epsilon_L)\,(\partial n/\partial x)|_{x=x_0}$, where a is the stripe width, and ϵ_L is the permittivity of the semiconductor. The width of the stripe can be evaluated from the condition that the drop of the electric potential equals the cyclotron energy:

$$a^2 \approx \hbar\omega_c\epsilon_L\left(e^2\,\frac{\partial n}{\partial x}\bigg|_{x=x_0}\right)^{-1}. \tag{8}$$

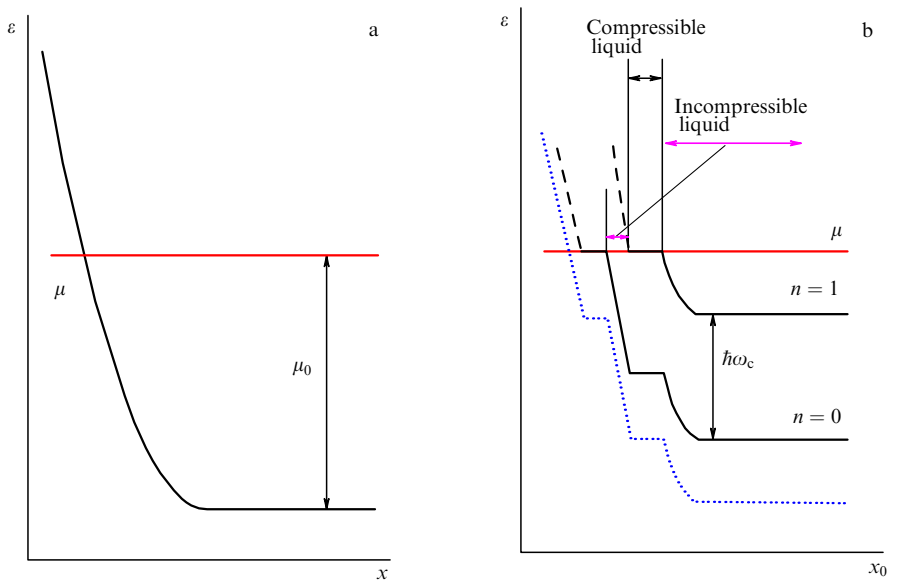

Figure 6. (a) Energy of the conduction-band bottom as a function of the coordinate in the case of a smooth potential and in the absence of a magnetic field; μ_0 is the chemical potential level counted from the bottom of the conduction band. (b) The energies of two Landau levels (completely filled in the bulk) as functions of the coordinate. Solid lines correspond to the part of the quantum level that is completely or partly filled, dashed lines mark nonfilled parts of the quantum energy levels. The dotted line shows the behavior of the electron-subband bottom.

The characteristic width of the incompressible electron liquid stripe in real samples amounts to 100 nm, and compressible-liquid stripes are an order of magnitude wider. The stripe system has been visualized in a number of experiments (see, for example, Ref. [21]). Electron states on a smooth edge significantly differ from the ones expected in the case of a sharp edge. Nevertheless the one-dimensional character of electron motion is preserved, and formula (7) together with the Büttiker technique [16] hold true.

3.6 Charge transport under the chemical potential level

In the physics of ordinary metals, we are used to the fact that the linear transport properties of a degenerate electron system can be expressed through the small perturbations of the distribution function in the vicinity of the chemical potential (see, for example, Ref. [22]). In an ideal two-dimensional electron system placed in a quantizing magnetic field, the charge transport on the chemical-potential level is possible only along the edge; however, this fact does not forbid a dissipativeless charge transport between the edges of the electron system below the chemical potential level. Attention to this fact was first drawn in Ref. [12].

The experiment can be performed using the structure shown in Fig. 7a. A two-dimensional electron gas has the shape of a ring (the Corbino geometry) that has its inner and outer radii in contact with the regions of an ordinary metal (not shown in the figure). A long thin solenoid with a controllable magnetic flux is placed inside the ring. A capacitor (C_0) and a voltmeter (V_1) are connected in parallel to the metallic contacts, and the whole system is placed in a quantizing magnetic field.

Variation of the magnetic flux $\Delta\Phi$ in the long thin solenoid causes a variation of the vector-potential azimuthal component at a radius r by a value of $\Delta\Phi/(2\pi r)$. The wave-function phase changes by $e\Delta\Phi/(c\hbar)$ per round trip along the azimuth of the ring. Providing

$$\Delta\Phi = \frac{ch}{e}\,, \tag{9}$$

the acquired phase equals 2π regardless of the radius; therefore, the electron system transforms into itself. Meanwhile, a single electron is brought into the electron system from one edge and is taken out of it from the other one at every quantum level, which is easy to verify by considering the quantized value of the Hall conductivity. The charge ΔQ crossing the radius r does not depend on the radius:

$$\Delta Q = \frac{ve^2}{h}\int_0^{2\pi} \mathrm{d}\phi \int_0^{\infty} \mathrm{d}t\, E(r)\, 2\pi r$$

$$= -\frac{ve^2}{hc}\int_0^{2\pi} \mathrm{d}\phi \int_0^{\infty} \mathrm{d}t\, \frac{\partial\Delta\Phi}{\partial t} = \frac{\Delta\Phi e}{c\hbar}\, ve\,. \tag{10}$$

Because the change in the magnetic flux $\Delta\Phi$ is not limited, any number of electrons can be transferred from one edge to the other below the chemical potential level.

Considering the real experiment [23], we will note in the first place that the long thin solenoid is in fact not needed at all, because one can vary the magnetic field B. In this case, the number of electrons entering the two-dimensional system will not be already equal to the number of electrons leaving it through the opposite contact. As shown in Ref. [23], if the initial electron filling factor is an integer, i.e., $n_s = \nu n_0(B)$ (where $\nu = 1, 2, \ldots$), then it will remain an integer even after the magnetic field changes. The voltage measured with the voltmeter in this case equals

$$V_1 = \Delta B\,\frac{\pi}{2}\,(r_1^2 + r_2^2)\,\frac{\sigma_{xy}}{cC_0}\,. \tag{11}$$

The results of the experiment for an increase and a decrease in the magnetic field are shown in Fig. 7b. One can see that the Hall conductivity demonstrates quantized values, although the quantizing accuracy ($\approx 1\%$) is not comparable to the accuracy of the Hall-resistance quantization. Straight lines corresponding to relation (11) are limited by the breakdown region related to the reverse tunneling of the electrons from the contact into the bulk of the sample [23]. It should be emphasized that the number of electrons transferred from one edge to the other in the real experiment indeed exceeded the initial number of electrons in the two-dimensional layer.

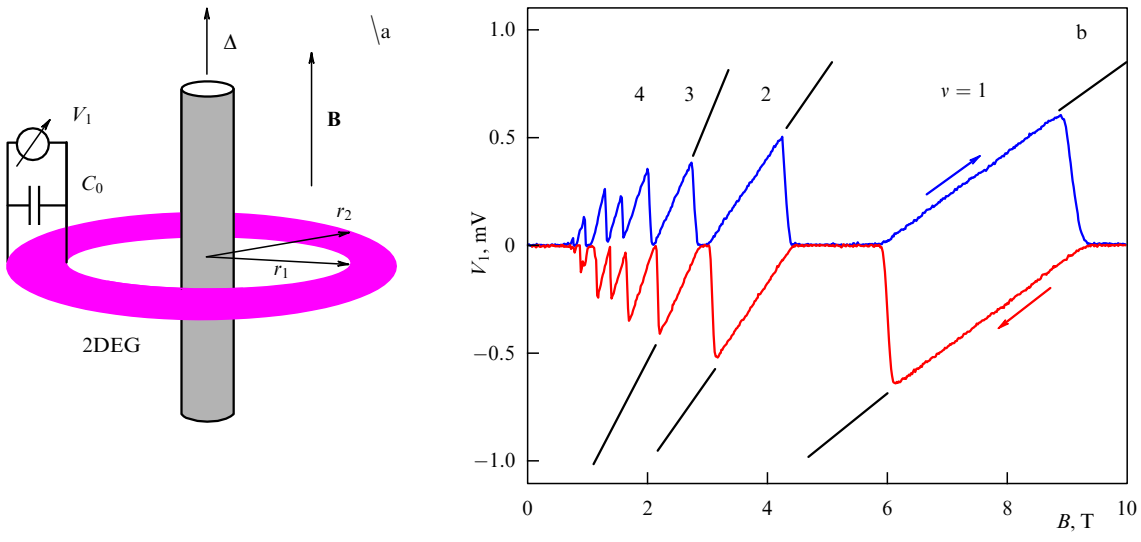

Figure 7. (a) Setup of the gedanken experiment on the observation of charge transport below the chemical potential level. (b) The results of a real experiment: $T = 30$ mK, $C_0 = 0.65$ μF, $2r_1 = 2.02$ mm, and $2r_2 = 3.9$ mm. Straight segments show the expected slopes.

3.7 Minimal width of the plateau

If the externally controlled parameter were the electron density, it would be impossible to observe the integer quantum Hall effect in an ideal (homogeneous and without scattering) electron system. Indeed, the dissipative component of the resistivity tensor would be zero, and the plateau for the Hall component would shrink into a point. In reality, we can control either the magnetic field or the gate voltage of the field-effect transistor.

As an example, let us consider the three-electrode system [24] shown in the inset to Fig. 8. Besides the gate separated from the two-dimensional electron system with a blocking barrier, the three-electrode system comprises a back electrode, tunnel connected with the two-dimensional electron gas having, therefore, the same value of the electrochemical potential. The number of electrons in the two-dimensional electron system is not fixed, because the system can exchange electrons with the back electrode, while the electroneutrality condition requires that the sum of the electron charges in the two-dimensional gas and in the back electrode be equal to the positive charge on the gate.

Figure 8 depicts the experimentally obtained dependence of the electron density of the two-dimensional electron gas on the gate voltage in the presence of the quantizing magnetic field. The dependence noticeably differs from the linear one observed in the case of a zero magnetic field. The experimental curve shows a barely visible plateau for the filling factor equal to unity and a well-pronounced plateau for the filling factor equal to two. These plateaus emerge because an ideal electron system has no states in the gap between the quantum energy levels. As long as the chemical potential level is crossing the gap, the electrons compensating for the variation of the positive charge on the gate are transferred to the back electrode. Correspondingly, the plateau width is expressed as

$$\Delta V_{\rm g} = \frac{x_{\rm g}}{x_{\rm w}} \frac{\Delta\mu(\nu)}{e}\,, \tag{12}$$

where $\Delta\mu$ is the jump of the chemical potential for the corresponding value of the filling factor (see Fig. 2). In a two-dimensional system, one can assume with a good accuracy that the distance between an electron layer and the back electrode is infinite ($x_{\rm g}$, $x_{\rm w} \to \infty$) and the plateau width in the gate voltage equals the jump of the chemical potential divided by the electron charge. This is the minimal width of the plateau.

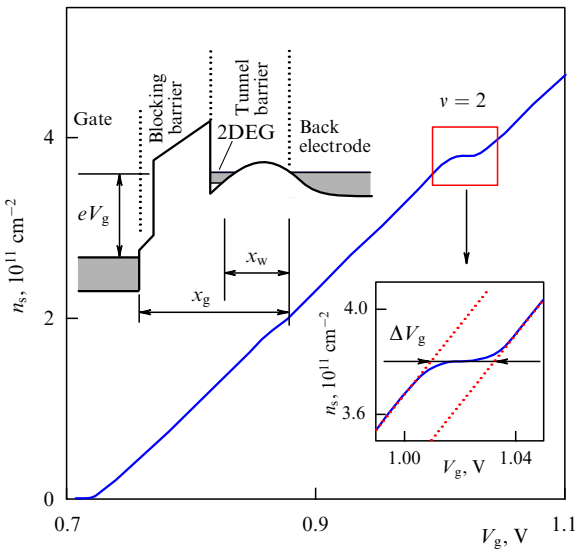

Figure 8. Dependence of the density of a two-dimensional electron gas on the gate voltage for $B = 16$ T, $T = 30$ mK in the three-electrode system shown in the inset to the top left corner of the figure.

It does not take great effort to calculate the minimal width of the plateau in the same model for the case of the scanning magnetic field:

$$\Delta B(\nu) = \frac{c\hbar\epsilon_L}{2e^2\nu(x_{\rm g} - x_{\rm w})} \frac{\Delta\mu(\nu)}{e}\,. \tag{13}$$

4. Electron system in a chaotic potential

4.1 Two limiting forms of a random potential

The experimental verifications of the predictions for an ideal electron system hold true whenever it is possible, in every specific case of a real sample, to neglect the existence of a random potential. On the other hand, as mentioned in Section 3, the presence of the random potential not only is no bar to the occurrence of the integer quantum Hall effect (as long as the characteristic time τ of the electron scattering is large: $\omega_{\rm c}\tau \gg 1$) but also plays a key role in the formation of a broad quantum plateau.

The characteristic spatial scale with which one should compare the scale of the random potential variation is determined by the magnetic length l, while the characteristic energy is specified by the cyclotron energy. Therefore, two limiting forms of a random potential are possible: the short-range one, if the variation of the electron potential energy on the magnetic length is comparable to the cyclotron energy or exceeds it, and the smooth one in the opposite case. In the first experiments (see, for example, Fig. 1), the investigated structures had the short-range random potential formed by impurities located close to the two-dimensional electrons and by surface roughnesses. Later on, structures with a smooth potential were also produced. It turned out that the integer quantum Hall effect is remarkably robust to the form of a random potential.

4.2 Density of states in a short-range potential

As an example, consider the influence of a small number of short-range impurities on the energy spectrum of the two-dimensional electrons in the vicinity of the lowest Landau level. We assume the density n_i of the impurities to be small in comparison with the density $n_{\rm s}$ of the electrons. We also assume the range of action of the impurity to be $b \ll l$, and its potential to be u. The appearance of the impurities causes two effects [25]: first, the localized states split from the quantum energy level, and second, the nonsplit states merge into a band. The total density of split and nonsplit states still equals $(2\pi l^2)^{-1}$.

The maximal energy for the splitting of a localized state can easily be estimated using the first-order perturbation theory:

$$\Delta = u\,\frac{b^2}{l^2}\,. \tag{14}$$

Localized states with smaller splitting energies will also emerge up to the boundary with the delocalized states on the energy level separated from the quantum energy level of an

ideal system by a value on the order of [25]

$$\delta = \Delta\left(\frac{b}{l}\right)^{1/(\pi l^2 n_i)} \ll \Delta\,. \tag{15}$$

It is interesting to note that introducing a single impurity with a small interaction radius leads to the localization of all the electrons in the two-dimensional system, although the shift in energy quickly decreases with increasing a distance between an electron and the impurity.

In the limit of a delta-like impurity potential, every impurity splits off only a single state of the quantum level. Such impurities, distributed chaotically over the plane, are used in the numerical modeling of a random short-range potential. It is assumed that the potential corresponds to white noise with the correlator

$$\langle V(\mathbf{r})\, V(\mathbf{r}')\rangle = V_0^2\delta(\mathbf{r}-\mathbf{r}')\,. \tag{16}$$

Here, the angle brackets stand for spatial averaging. A system of delta-like impurities with a relatively small concentration $n_i < (2\pi l^2)^{-1}$ cannot simulate such a potential at all, because the number $(2\pi l^2)^{-1} - n_i$ of single-electron states can be represented as a linear combination of initial wave functions in such a way that every impurity will be occupied by a node of the wave function. Correspondingly, the center of every quantum level would be taken up by a delta-like peak of the density of states. For modeling a potential with correlator (16), one would need an impurity concentration exceeding the number of states on a single quantum level by 40-fold [26].

Assuming the set of the short-range impurities to be electroneutral (that is, with equal number of impurities for $u < 0$ and $u > 0$) and distributed in u, we obtain the well-known textbook image of the density of states displayed in Fig. 9a. In the case of a potential with correlator (16), only a single extended state will remain on every quantum energy level.

If the level of the chemical potential is located in the band of localized states (Fig. 9a), the dissipative conductivity component exhibits an activation behavior that is replaced by the variable range hopping as the distance from the center of the quantum level increases. If the chemical potential is located in the band of delocalized states, the dissipative conductivity component takes values typical for metals. Therefore, the variation in the chemical potential position over a broad range results in a chain of metal–insulator transitions.

The width and the position of the band of delocalized states can be derived, for example, from activation energy measurements (Fig. 9b). From the data shown in the figure, it follows immediately that the chaotic potential in the investigated sample is not symmetric, and the band of delocalized states does not correspond to a half-filled quantum energy level.

The presence of a broad band of localized states (the mobility gap) was utilized in Ref. [12] to prove the connection between the quantization of the Hall conductivity and the gauge invariance in a system with disorder. Indeed, because an adiabatic variation of the magnetic flux through the thin solenoid (Fig. 7a) cannot give birth to delocalized electron–hole pairs, the change in the magnetic flux by a value given by relation (9) must lead, as in the ideal case, to a transfer between the edges of an integer (or zero) number of electrons.

4.3 Floating up of extended states in a short-range potential

The idea that the extended states in a weak magnetic field would shift upwards in energy and move to infinity as the field decreases [28] is based on a prediction that follows from the scaling hypothesis [29]. This prediction states that in a zero magnetic field even a weakly disordered two-dimensional system of noninteracting electrons has to be an insulator at a zero temperature regardless of the electron density. On the other hand, according to Ref. [30], delocalized states have a topological protection and cannot disappear with a decrease of the magnetic field. A picture appears, schematically shown in Fig. 10a, where the bright stripes represent the extended states, and the dark ones represent the localized states. Plateaus are expected to form in the conductivity σ_{xy}, whose center positions are marked in Fig. 10a by arrows. The numbers alongside the arrows indicate the values of the Hall conductivity in normalized units. In weak magnetic fields, $\omega_c\tau < 1$, the plateau sequence is reversed with respect to the case of a strong quantizing magnetic field.

The attractiveness of the picture described led to a series of attempts went into experimental observation of the floating up of the delocalized states (see, for example, Refs [31–34]). It is firmly established that the extended states do not follow the line in the plane (B, n_s) along which the maximum of the

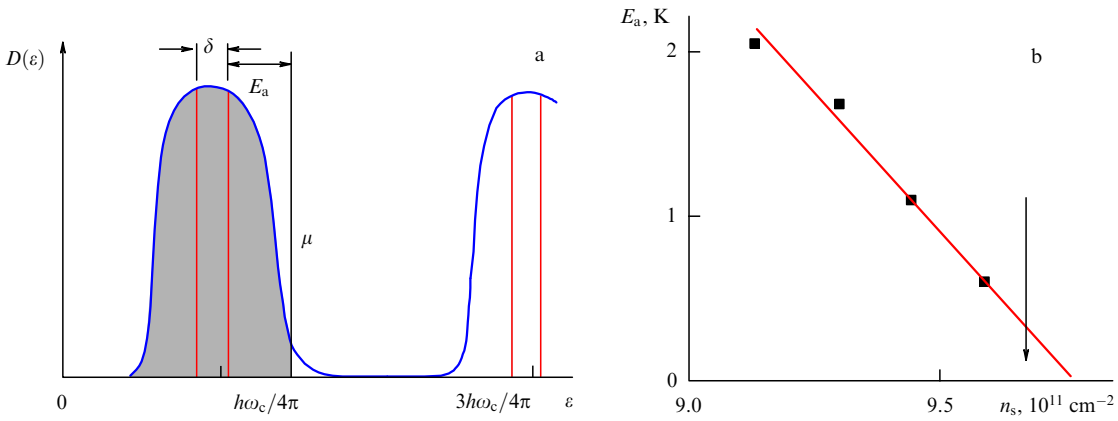

Figure 9. (a) Schematic dependence of the density of states D on energy ε in a quantizing magnetic field in an electron system with a short-range chaotic potential: E_a is the activation energy, and δ is the band width of delocalized states. (b) The dependence of the activation energy on the electron density for the sample GaAs/AlGaAs placed in a normal magnetic field of 16 T [27]. The arrow indicates the electron density corresponding to the filling of 2.5 quantum levels.

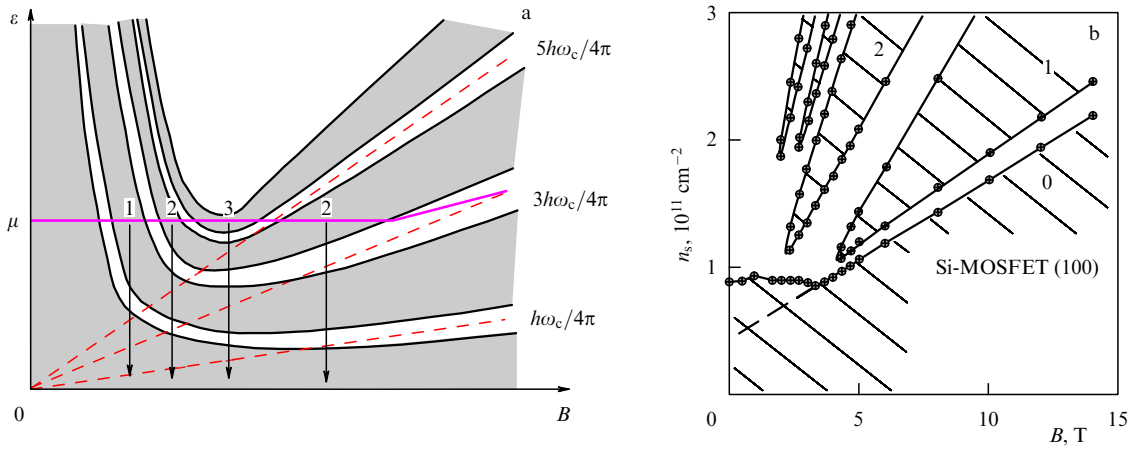

Figure 10. (a) Schematic drawing illustrating the floating up of the delocalized states of the three lowest quantum levels. (b) The phase diagram in the (B, n_s) plane obtained experimentally for an electron gas in Si-MOSFET (100) at $T = 30$ mK. The numbers 0, 1, and 2 indicate the number of the extended states below the Fermi level if this level is located within the boundaries of the corresponding shaded area.

density of states should move in an ideal sample. This statement is illustrated in Fig. 10b. One can clearly see that the extended states do not go below some boundary where oscillations take place, and merge, as they approach $B = 0$, into a metallic state typical for a large electron density. The disappearance of the bands of localized states in a weak magnetic field did not allow the observation of additional plateaus in the Hall conductivity. In several studies (see, for example, Ref. [32]) a weak increase in the electron concentration, corresponding to a maximum of σ_{xy}, was observed as the magnetic field weakened, but it remained unclear whether this effect is related to the oscillation of the boundary between the metallic and insulating phases.

In fact, the absence of clearly pronounced effects related to the floating up of the delocalized states is not surprising. Indeed, the presence of the chaotic potential leads, in the case of a small electron density, to the localization of the charge carriers and to the Anderson metal–insulator transition at some critical electron concentration. In the region of the metallic conductivity there is a temperature-dependent correction related to the electron interference, which decreases the conductance by a value on the order of $(e^2/h)\,|\ln T|$. It is supposed that, as the temperature tends to zero, the correction reaches the scale of the initial conductance of the two-dimensional electron system, and the electrons localize at this temperature. A typical value of the dimensionless conductance of an average-quality electron system reaches ~ 100 in a metallic state; therefore, localization requires a temperature of about $\exp(-100)$ and a linear size of the system of $\sim \exp 100$. Neither of these conditions is realizable; therefore, all one can have in a real situation is a weak logarithmic shift of the Anderson-transition point to higher electron density. In other words, under real conditions there is no significantly wide region for the observation of the floating up of the states.

Another problem is the disappearance of the bands of localized states in weak magnetic fields, which is revealed in almost all experimental work but so far has elicited no comments on it in theory. [1]

[1] Recently, numerical simulations have appeared that possibly point to the completely opposite behavior of the quantum levels with a magnetic field weakening: antilevitation (see Ref. [36]). There is no experimental evidence so far of antilevitation.

4.4 Two-parameter scaling

As we discussed in Section 4.3, part of the electrons in an infinite electron system is localized in the presence of short-range scatterers. It is natural to pose a question: how will the dimensionless conductances σ_{xx} and σ_{xy} behave themselves in finite-sizes samples? This problem was considered within the framework of the scaling hypothesis. It is assumed that the state of the system is uniquely defined by two components σ_{xy} and σ_{xy} of the conductivity tensor; therefore, the variation of these components with a change in the electron system size is assigned by the conductance components themselves [35, 37, 38]:

$$\frac{\partial\sigma_{xx}}{\partial\ln L} = \beta_{xx}(\sigma_{xx},\sigma_{xy})\,, \quad \frac{\partial\sigma_{xy}}{\partial\ln L} = \beta_{xy}(\sigma_{xx},\sigma_{xy})\,. \tag{17}$$

In the case of a chaotic short-range potential with the correlator (16) in the region $\sigma_{xx} > 1$, the following expressions for the functions β_{xx} and β_{xy} have been obtained [38]:†

$$\beta_{xx} = -\frac{1}{2\pi^2\sigma_{xx}} - D\sigma_{xx}\exp(-2\pi\sigma_{xx})\cos(2\pi\sigma_{xy}),$$

$$\beta_{xy} = -D\sigma_{xx}\exp(-2\pi\sigma_{xx})\sin(2\pi\sigma_{xy})\,, \tag{18}$$

where D is an unknown constant.

Excluding the parameter L from the solutions of the system of equations (17), (18), it is convenient to depict these solutions as flow lines in the $(\sigma_{xy},\sigma_{xx})$ plane (Fig. 11a). First, let us discuss the formal consequences from equations (18). For large values of σ_{xx}, the Hall component of the conductance does not renormalize, and all flow lines in this region are parallel to the y-axis. Significant deviations from such behavior occur at $\sigma_{xx} \approx 1$. The flow lines corresponding to integer values of σ_{xy} remain vertical in this region as well, reaching the zero value of σ_{xx}, and for half-integer values of the Hall conductance they go vertically down to some value σ_{xx}^{c}, at which point β_{xx} turns to zero. For other values of the Hall conductance, as the dissipative component of the conductance decreases, the flow lines tend to get to one of

† Equation (18) is written out here in the form adopted in paper [38]. Recently (see the paper by Pruisken A M M, Burmistrov I S *JETP Lett.* **87** 252 (2008)), a misprint was revealed in Ref. [38]. Upon correction, the σ_{xx}-dependences of the terms involving σ_{xy} in both formulas of Eqn (18) became identical to those in Eqn (19). Moreover, the coefficient D was calculated as equal to ≈ 16.5. (*Author's note added in English proof.*)

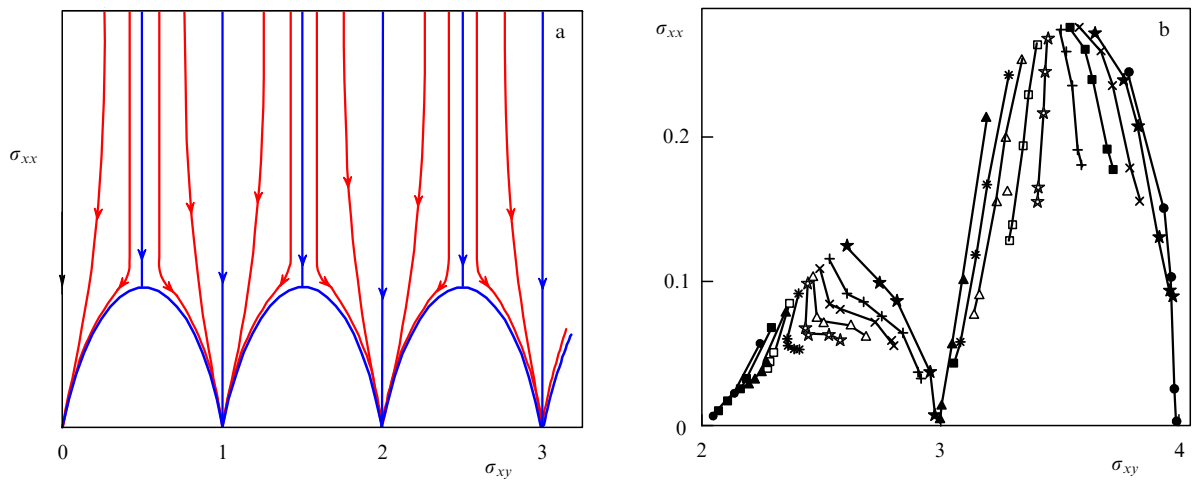

Figure 11. (a) Expected diagram of the flow lines in the $(\sigma_{xy}, \sigma_{xx})$ plane. (b) The experimentally obtained diagram of the magnetic flow lines for a two-dimensional electron gas in Si-MOSFET(100), $n_s = 4.2 \times 10^{11}$ cm^{-2}. (Adopted from Ref. [39].)

the points $(i, 0)$, where i is an integer. At every critical point $(i + 1/2, \sigma_{xx}^0)$, the flow lines split into pairs with different directions, asymptotically approaching some limiting curve (bold bow-shaped curve in Fig. 11a). Let us stress that the picture proposed is partially based on the extrapolation of rigorous solution (18) to the region where this solution is not valid.

Theoretical treatment of the problem [35, 37, 38] and the above-devised equations refer to a gas of noninteracting spin-polarized electrons. Two natural questions arise in this connection: why is a variation in the conductance with a change in the size expected at all for large dissipative conductances, and why is the corresponding correction to σ_{xx} negative and proportional to $\ln L$? The answer sounds a bit paradoxical: the correction is related to the weak localization. The leading weak-localized term, often explained by 'hand-waving arguments', is known to be suppressed with the introduction of a weak magnetic field normal to the plane of the two-dimensional gas. This term is related to the interference of the electron waves returning to the initial point in a loop path as a result of multiple scattering. Besides this simplest path, one can specify other ones, for example, paths in the form of a figure eight that are more stable under magnetic field suppression.

In real two-dimensional electron systems, it is impossible to neglect the electron-electron interaction. In this case [40], the two-parameter scaling holds true if the functions β_{xx} and β_{xy} are modified:

$$\beta_{xx} = -\frac{2}{\pi} - D_1 \sigma_{xx}^2 \exp(-2\pi\sigma_{xx}) \cos(2\pi\sigma_{xy}),$$
$$\beta_{xy} = -D_1 \sigma_{xx}^2 \exp(-2\pi\sigma_{xx}) \sin(2\pi\sigma_{xy}), \qquad (19)$$

where $D_1 = 64\pi/e \approx 74.0$.‡ All the discussions above, including the one referring to the logarithmic correction to σ_{xx} for large dissipative conductances and to the structure of flow lines, remain valid for equations (19).

The choice of the flow diagram line in the experiment can be made by selecting three parameters: the electron density n_s, the magnetic field B, and the amplitude V_0 (or τ) of the chaotic potential. It seems that one can proceed from any point of the $(\sigma_{xy}, \sigma_{xx})$ plane. Let us consider this problem in detail. For this purpose, we will fix the electron concentration and for a start we will restrict ourselves to the case of $\omega_c\tau \leqslant 1$. Classical expressions for the conductivity components limit us under these conditions to the upper quadrant of a circle:

$$(\sigma_{xy}^0)^2 + \left(\sigma_{xx}^0 - \frac{\sigma_0}{2}\right)^2 = \frac{(\sigma_0)^2}{4}, \qquad (20)$$

where σ_0 is the value of the conductivity in a zero magnetic field, $\sigma_0 \geqslant \sigma_{xx}^0 \geqslant \sigma_0/2$, and $0 \leqslant \sigma_{xy}^0 \leqslant \sigma_0/2$. For the reasons discussed above (see also Sections 4.2, 4.3), the choice of large initial values σ_{xx}^0 will not lead to a considerable shift down along the flow line; therefore, a very limited area σ_{xx}^0, $\sigma_{xy}^0 \leqslant 2, 3$ of the plane is available under such conditions at the beginning.

In the opposite limiting case of $\omega_c\tau \gg 1$, the initial choice of the point in the $(\sigma_{xy}, \sigma_{xx})$ plane is determined by the applicability limit of the self-consistent Born approximation, in which the initial area is determined by the relations

$$[\sigma_{xx}^0]^{\max} = \frac{2e^2}{\pi h}\left(i + \frac{1}{2}\right), \quad i = 0, 1, 2, \ldots, \quad \sigma_{xy}^0 \leqslant \sigma_0. \qquad (21)$$

In the experiment, it is not the size dependence of the conductivity but the temperature one that is investigated. It is assumed that the size of the interference area is determined by the dephasing length $L_\phi(T)$ or by the linear size L_{ee} of the electron–electron interaction region. The macroscopic sample has much bigger sizes, and the conductance is automatically averaged over many samples with the size $L(T)$. Both characteristic sizes have a power dependence on temperature. The flow line diagrams are presented in a series of publications (see, for example, Refs [3, 39, 41–43]).

An example of an experimentally plotted flow diagram is given in Fig. 11b. Every line in the diagram corresponds to a fixed filling factor at a constant electron density, which means that the quantities n_s and B are fixed. The chaotic potential is also assumed not to depend on the temperature in the interval from 0.3 K to 1.2 K, where the measurements were performed. The main experimental conclusion is that there is a qualitative correspondence between the observed flow diagrams and their theoretical predictions: above all, one can

‡ $D_1 \approx 13.5$ in the case of the Coulomb interaction (see Pruisken A M M, Burmistrov I S *JETP Lett.* **87** 252 (2008)). (*Author's note added in English proof.*)

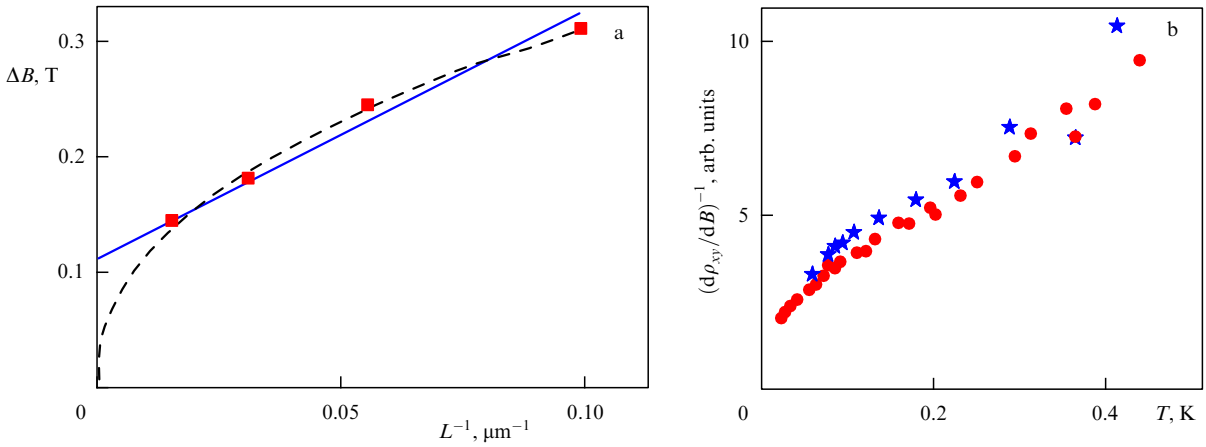

Figure 12. (a) Dependence of the peak width on the sample size for the 2–3 transition (the transition between the plateaus with the corresponding numbers in the Hall resistance). (Adopted from Ref. [50].) (b) The dependence of the inverse slope of the Hall resistance, $(d\rho_{xy}/dB)^{-1}$, at the 1–2 transition on the temperature for a two-dimensional electron gas in a strongly disordered GaAs/AlGaAs heterostructure. (According to the data from Ref. [51]).

indeed see the motion of the flow lines from top to bottom, part of the flow lines is directed to the points $(i + 1/2, 0)$, a limiting bell-shaped curve can be traced along which the experimental points approach the abscissa, and, finally, on every bell-shaped curve one can find a point separating the right- and left-directed flow lines.

There are also significant deviations from the theoretical predictions. Above all, these comprise the nonuniversality of the vertical size of the bell-shaped curves measured both on a single sample and on different samples, the unexpected bending of the flow lines near the half-integer values of the Hall conductance, and the absence of symmetry with respect to the half-integer σ_{xy}. The last circumstance significantly differs from one sample to another and can actually be related to the chaotic potential asymmetry.

The only obvious exception to the overall series of experimental results are those of Ref. [44], where almost complete coincidence of the bell-shaped curves is observed for two intervals in σ_{xy}: (0, 1) and (1, 2). Based on the results of this work, it was assumed in further theoretical models [45] that the limiting bell-shaped structure represents a semicircle, although in the original data the points do not approach the semicircle but move away from it as the temperature decreases.

Apparently, the result of Ref. [44] should be treated as accidental, because in all experiments where a sharp increase in ρ_{xx} was evidenced on some ρ_{xy} plateau [46–48] the observed bell-shaped curves had the form of a semicircle with a non-universal radius depending on the plateau number. The accidental nature of the semicircle observation was also confirmed by the results of recent simulations [49].

Another method for processing experimental results allows one to estimate the degree of applicability of the scaling theory predictions to the real situation in the two-dimensional electron systems investigated. This method is based on a set of assumptions, namely:

(1) as in the theory, the chaotic potential appears as a white noise;

(2) in an infinite-sized sample, unlike in the picture depicted in Fig. 9, at zero temperature there is only one delocalized state on every quantum level at energy ε_i;

(3) the measurement domain is chosen in such a way that the flow lines adjoin the bell-shaped curve;

(4) the measurements are performed in the region where the density of states can be assumed to be constant.

Measurements of one of the conductance components have been performed,[2] for example, σ_{xx}, on identical samples of different size L at such a low temperature that the temperature dependence of the conductance becomes saturated [50]. According to the above assumption 3, σ_{xx} is the function of only one variable, the ratio L/ξ, where $\xi \propto |\varepsilon - \varepsilon_i|^{-\nu}$ is the localization length of an electron with the energy ε. The width of the peak in the conductance dissipative component at a fixed height $\Delta B(L)$ is also measured. Taking into account assumption 4, one obtains $\Delta B \propto L^{-1/\nu}$.

The most convincing and, as the authors of the publication believe, the most accurate results were obtained by Koch et al. [50], where the above-described program was realized. The experimental points from that work are presented in Fig. 12a. If one utilizes only the experimental points, the multitude of different lines with a cut-off on the ordinate can be drawn as fitting curves, the simplest one being the straight line shown in Fig. 12a. In analyzing their results, the authors of Ref. [50] have added, without informing the readers, the point (0, 0) to the experimental points, in compliance with the above assumption 2, and used as the optimal fit the curve corresponding to $\nu = 2.3 \pm 0.1$ (dashed line in Fig. 12a). The last value agreed wonderfully with the theory [52] existing at the time of the publication, as well as with the results of numerical simulations [53]. However, the theory did not refer to the short-range potential, and the numerical modeling was later corrected in such a way that within the limits of the specified accuracy the experimental results did not coincide with the theoretical ones any more [54].

Similar measurements of the characteristic width of the σ_{xx} peak or the steepness of the slope of ρ_{xy} at the transition between the plateaus as the functions of temperature have been performed in many experimental studies (a detailed description of the experiments can be found in review [55]). The interpretation of such measurements is additionally complicated by the fact that the temperature dependence of the length L_T, playing the role of the sample size, is itself known only tentatively. Nevertheless, the available experi-

[2] The components of the resistivity tensor are often used in processing the experimental results.

mental data rather point to the presence of a band of delocalized states in the samples investigated (Fig. 12b). This conclusion is also supported by the measurements of the peak width of the dissipative conductance as a function of frequency [56].

As evidenced by the foregoing, many predictions of the theory are either not confirmed by experimental results at all or confirmed qualitatively. Nevertheless, it certainly follows from both the theory and experiment that in a quantizing magnetic field in the presence of the short-range chaotic potential, as a result of interference effects and electron–electron interactions the electrons localize within regions significantly exceeding the magnetic length (up to $10^4 l$ in experiments [50]), and the size of a localization region increases dramatically as the electron energy approaches the energy of the delocalized states.

4.5 Smooth potential

The motion of every electron in a smooth potential can be treated as the motion of its guiding center along the equipotential line. (This statement follows from the fact that the work done by Lorentz force is zero.) In a symmetrical smooth potential (Fig. 13a) there is a set of minima and maxima separated by saddle points. Equipotential lines passing through the saddle points form a grid with the cells determining the spatial scale of the potential and composing an infinite cluster. All other equipotential lines surrounding the minima and maxima are enclosed and correspond to localized electrons.

In a fixed magnetic field, as the electron concentration increases, first the minima of the potential are filled and the chemical potential level finds itself in the band of localized states, then the chemical potential crosses the energy level of the infinite cluster and again goes to the band of localized states, whose paths surround the potential maxima.

The reason behind the emergence of the quantized values of the Hall conductance was revealed in Ref. [57]. In an electric field parallel to the plane, the picture of the equipotential lines significantly changes (Fig. 13b), because the saddle points acquire the energy difference $\Delta W = e\mathbf{ER}$, where $\mathbf{R}$ is the radius vector connecting the neighboring saddle points. Strips of the extended states emerge (dark regions in Fig. 13b) directed on average normally to the electric field. According to the consideration of Section 3.4, the current $\Delta I = \Delta W(e/h)$ is carried along the stripe of the extended states if they are filled. Summing all the currents within a unit length and over all filled quantum levels, we obtain the expression $\sigma_{xy} = ve^2/h$, where, as in formula (1), v is the number of occupied quantum levels.

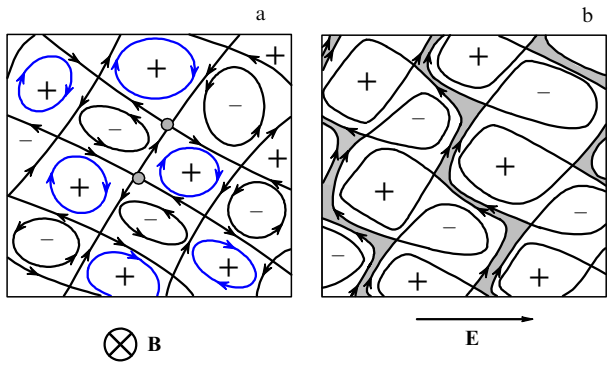

Figure 13. (a) Schematic image of a smooth chaotic potential in the absence of an external electric field. Signs + and − mark the maxima and minima of the potential, respectively. The arrows indicate the motion of the guiding center. (b) Image of a smooth chaotic potential in the presence of an electric field. Dark color marks the regions of the extended states that carry current.

This model has an obvious disadvantage: the transition region between the plateaus depends on the electric field strength. Moreover, using the local relation between the current and the electric field is possible only on scales significantly exceeding the size of the percolation grid.

4.6 Screening of a chaotic potential

The chaotic potentials discussed in Sections 4.1–4.4, generally speaking, do not coincide with the initial potential that existed in the absence of the two-dimensional electron gas. In the long-wave limit ($q \to 0$), linear screening by the electron system is determined by the effective permittivity

$$\epsilon(q) = \varepsilon_L \left(1 + \frac{q_s}{q}\right), \tag{22}$$

where q_s is the inverse screening radius:

$$q_s = 2\pi e^2 \frac{\partial n_s}{\partial \mu} \frac{1}{\varepsilon_L},$$

$D_{th} = \partial n_s/\partial\mu$ is the thermodynamic density of states, and the chemical potential μ is counted off from the bottom of the two-dimensional subband.

One can conclude from Eqn (22) that, if the density of states on the chemical potential level is zero, then under the conditions of the quantum Hall effect at zero temperature, the emergence of the two-dimensional electron gas will not modify the smooth potentials with a small amplitude. This conclusion is not correct though [58]. Indeed, the electric field shifts the minimum of the magnetic parabola (see Section 3.1). Consequently, the second derivative of the potential with respect to the coordinate determines the variation of the electron density, which leads to the peculiar potential screening.

At a finite temperature, occupied electron states appear on the upper quantum level and, correspondingly, empty ones on the lower level. The number of the former and the latter depends on both the temperature and the chemical potential position; therefore, the thermodynamic density of states happens to be finite even in the ranges where it was initially zero. An additional temperature-dependent screening shows its worth.

Especially interesting and practically important is the case of nonlinear screening, where the characteristic amplitude of the smooth chaotic potential is comparable to or even exceeds the energy gap between the neighboring quantum energy levels [59]. We will start with a potential having a relatively small amplitude, $|U| \leqslant E_e - E_f$, where E_e and E_f are, respectively, the energies of the empty and filled neighboring quantum levels in an electron system without disorder. The thermodynamic density of states defined on a spatial scale significantly exceeding the characteristic scale of the chaotic potential is a function of the quantum level width, the latter depending on the screening and, consequently, on the thermodynamic density of states. To derive these quantities, one has to solve the set of equations [60]

$$D_{th} = D_{th}(\Gamma, \mu), \quad \Gamma = \Gamma\left(\Sigma_q \frac{U_q}{\epsilon_q}\right), \tag{23}$$

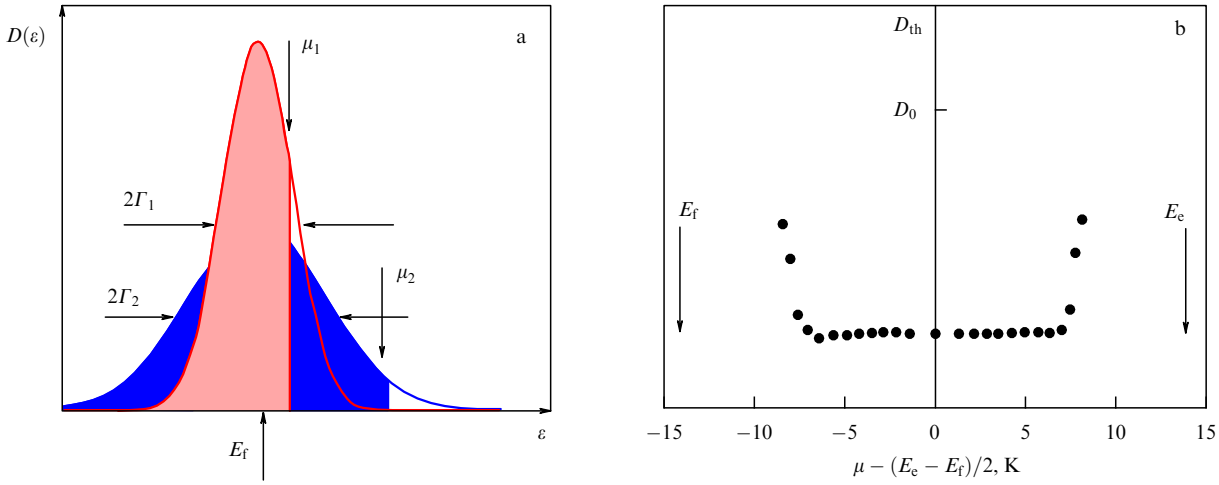

Figure 14. (a) Illustration of the solution to the set of equations (23) for two values of the chemical potential, μ_1 and μ_2, $\mu_2 > \mu_1$, and $D(\varepsilon) = (\partial n/\partial\varepsilon)_\mu$ being the one-particle density of states. (b) Thermodynamic density of states $D_{\rm th}$ as a function of energy, according to activation-energy measurements in Si-MOSFET (100) in the vicinity of the filling factor $\nu = 8$ for $B = 6.7$ T, and D_0 being the thermodynamic density of states in a zero magnetic field (taken from the results of Ref. [61]).

where $D_{\rm th}$ is the thermodynamic density of states, Γ is the width of the quantum level, and ϵ_q is the dielectric constant.

The solution is qualitatively illustrated in Fig. 14a. As the chemical potential moves away from the midpoint of the level $E_{\rm f}$, the width Γ of the quantum level increases proportionally to $|E_{\rm f} - \mu|$. Already in the first experiments [61, 62], this dependence manifested itself (Fig. 14b) as the disappearance of the influence of the chemical potential position on the value of the measured thermodynamic density of states in the vicinity of an integer filling factor. It should be noted that the thermodynamic density of states was replaced in the processing of the results of these experiments by the quantity $\partial E_{\rm a}/\partial n_{\rm s}$, which is correct only if the boundary between the localized and delocalized states does not itself depend on the width of the quantum level. More detailed measurements of the thermodynamic density of states with the help of the experimental technique discussed in Section 5 and a comparison of the experimental and theoretical results were performed in Ref. [60].

Let us proceed now to the consideration of the case where the amplitude of the smooth potential significantly exceeds the energy gap. We will assume that the short-range components of the potential are completely absent, so that without a smooth potential the electron spectrum would be given by a set of delta-functions. In the regions of electron integer filling, as discussed above, the screening of the seeding potential by the electron system is weak and can be neglected. But, wherever the quantum level reaches the chemical potential (in the regions of partial filling), electrons or holes fully screen all the gradients of the potential, and the quantum energy level becomes flat. The spatial behavior of the electron spectrum is qualitatively demonstrated in this case in Fig. 15a, and the single-particle density of states is shown in Fig. 15b. The maxima of the single-particle density of states do not coincide any more with the ones expected for an ideal electron system and, being linked to the chemical potential level, move together with it [63].

The picture introduced above has not been directly proved so far, but there is indirect evidence of its validity [64].

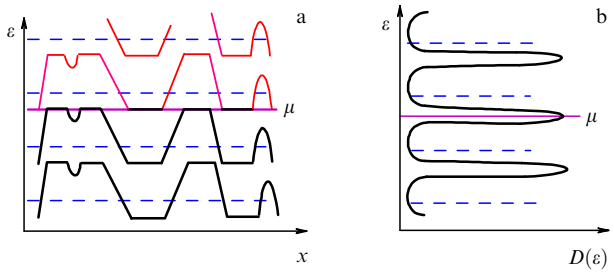

Figure 15. (a) Schematic of the spatial behavior of the quantum levels in a high-amplitude chaotic potential. Dashed horizontal lines indicate the energies of the quantum levels in an ideal (without the chaotic potential) electron system. Bold lines correspond to partly or fully filled quantum levels. (b) Single-particle density of states, corresponding to figure a.

5. Effects caused by electron–electron interactions

5.1 Negative thermodynamic density of states

Far better opportunities for the investigation of the thermodynamic density of states are given by three-electrode systems, such as those shown in the inset to Fig. 8. Besides the gate and the two-dimensional electron gas, these systems contain a metallic built-in electrode (back electrode), with the electrochemical potential coinciding with the electrochemical potential of the two-dimensional electrons (Fig. 16).

Let a positive charge ΔQ be added to a unit area of the gate in such a three-electrode system which was initially in the equilibrium state. The additional charge $\Delta Q_{\rm 2DEG}$ having appeared in the two-dimensional electron gas can be found from the solution of a standard electrostatic problem:

$$\Delta Q_{\rm 2DEG} = -\frac{\Delta Q}{1 + (D_{\rm th} x_{\rm w} 4\pi e^2/\epsilon_L)^{-1}}\,, \qquad (24)$$

where ϵ_L is the static permittivity.

If the thermodynamic density of states is positive and finite, the two-dimensional electron gas does not completely screen the normal component of the electric field

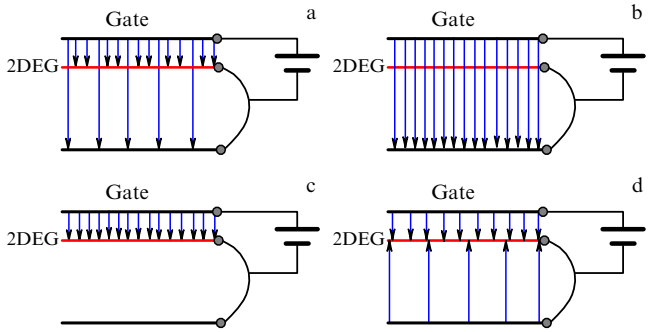

Figure 16. Distribution of the additional electric field in a three-electrode system in the case of a positive charge ΔQ added to the gate. (a) Finite thermodynamic density of states in the two-dimensional electron system. The electric field E at the gate exceeds the field E_p penetrating through the two-dimensional electron gas (2DEG). (b) The case of zero thermodynamic density of states: $E = E_p$. (c) The case of infinitely large thermodynamic density of states: $E_p = 0$. (d) The case of negative thermodynamic density of states: E_p is directed opposite to E.

($\Delta Q_{2DEG} < \Delta Q$), and the electric field penetrates through it (Fig. 16a). At a zero thermodynamic density of states one has $\Delta Q_{2DEG} = 0$ (Fig. 16b), while at infinitely large value of D_{th}, complete screening takes place (Fig. 16c).

All three cases are presented in Fig. 17a. In a zero magnetic field, the capacity of the three-electrode system is less than the geometrical capacity determined by the distance between the gate and the two-dimensional electron gas. In a quantizing magnetic field, the capacity at the maxima of the density of states coincides with the geometrical one, while at the deepest minima it decreases to the values determined by the distance between the gate and the back electrode.

A closer look at Fig. 17a gives evidence that in some regions the measured capacity exceeds the geometrical one. This effect is more pronounced in Fig. 17b (taken from Ref. [66]), where the authors measured the derivative of the electric field penetrating through the two-dimensional layer with respect to the electric field in the space between the gate and the electron gas. It was discovered that these fields are oppositely directed, as shown in Fig. 16d. The results of these and similar experiments [67] should be interpreted as the discovery of the negative thermodynamic density of states depending on the filling factor.

A question immediately arises: how can an electron system with a negative thermodynamic density of states, i.e., with a negative compressibility, be stable? The answer is that the electron system considered here is not closed. Indeed, it interacts with the compensating charge, the electric field of which is responsible for maintaining the stability.

There are no doubts that the negative thermodynamic density of states is caused by the interaction between the electrons. The main contribution is made by the electron exchange interaction. Indeed, the exchange energy in a fully spin-polarized system per electron on the lowest quantum level has the scale determined by the average distance between the electrons [68].

The variation of the chemical potential consists of two components: the change in the energy of noninteracting particles (which is close to zero at the maximum of the density of states), and the change in the negative interaction energy. Therefore, the thermodynamic density of states can be estimated, taking into account the electron–hole symmetry, as follows:

$$\left(\frac{\partial n_s}{\partial \mu}\right)^{-1} = -\frac{e^2}{l\epsilon_L}\, \nu^{1/2}(1-\nu)^{1/2}\,. \qquad (25)$$

Qualitatively, equation (25) is in good agreement with the results given in Fig. 17b. A quantitative agreement [65] is achieved by using the semiempirical expression [69] for the electron interaction energy. The corresponding curve (dotted curve in Fig. 17b) agrees very well with the experimental results for filling factors of less than 0.5. This inference is not very surprising, because it is discovered that for higher filling factors the spin-polarization is not perfect (see, for example, Ref. [70]).

5.2 Spin gap. Skyrmions

The most convenient objects for the study of the energy gap caused by the flipping of the spin projection onto a magnetic field turned out to be GaAs/AlGaAs heterojunctions and quantum wells. Based on them, high-quality structures were

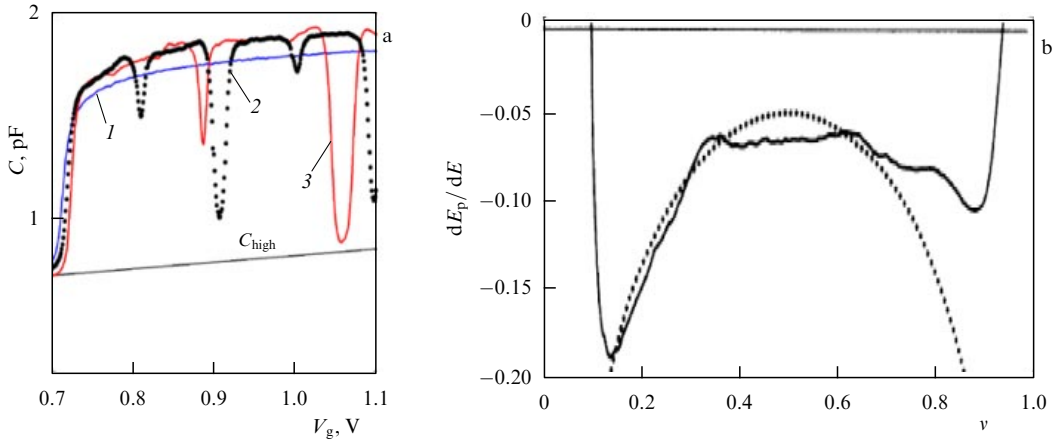

Figure 17. (a) Capacity of a three-electrode structure (see the inset to Fig. 8) as a function of voltage at the gate in the magnetic fields $B = 0$ (curve *1*), $B = 5$ T (curve *2*), and $B = 9$ T (curve *3*). The temperature is $T = 30$ mK. The straight line indicates the high-frequency limit of the capacity C_{high}. (b) The derivative of the electric field penetrating the two-dimensional layer with respect to the electric field in the space between the gate and the electron gas versus the filling factor at $B = 7.5$ T, and $T = 1.2$ K. The dashed curve shows the result of calculations according to Ref. [65]. (Data taken from Ref. [66].)

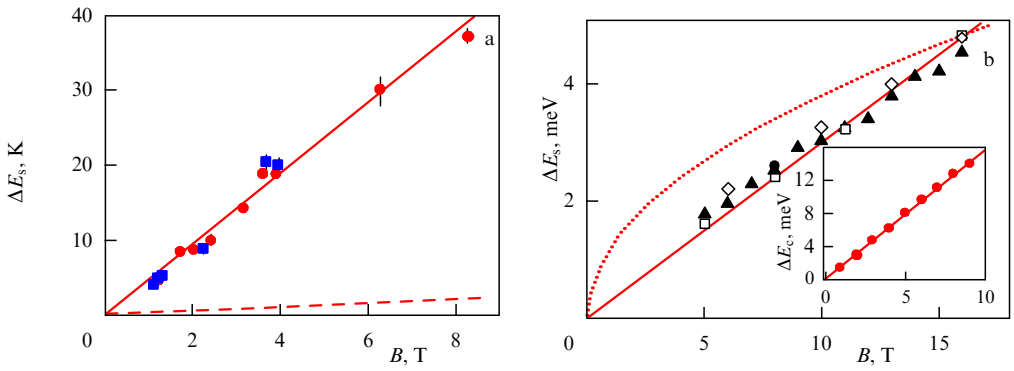

Figure 18. (a) Spin energy gap found from the activation energy. Circles correspond to $\nu = 1$, and squares to $\nu = 3$. The dashed line shows the Zeeman splitting. (Data taken from Ref. [71].) (b) The jump of the chemical potential at $\nu = 1$, measured using magneto-capacitive methods; $T = 30$ mK. The inset shows similar measurements for the cyclotron gap. The dotted curve corresponds to the dependence $\Delta E_s \propto B^{1/2}$. (Data taken from Ref. [24].)

created with a simple energy spectrum and weak spin-orbit interaction. Already in the first experiments on the activation-energy measurement for the filling factor $\nu = 1$ (Fig. 18a), it was demonstrated that the observable energy gap significantly exceeds $\mu_B g B$, with g-factor values typical for a bulk material.

This result is quite expected, because the spin-flip is related to the change in the exchange energy, significantly exceeding the Zeeman energy [72, 73]. Indeed, a thermal excitation creates pairs consisting of an electron with a negative magnetic moment projection onto the external magnetic field and a vacancy on the initially filled quantum level. Such formations can carry a current only if the electron with the flipped spin projection and the vacancy move independently, i.e., they are far away from each other — in the ideal case, infinitely far. The electron–vacancy pair (see Section 3.1) has an infinitely large momentum; therefore, the expected activation energy for the filling factor $\nu = 1$ is defined as

$$\Delta E_a = \frac{1}{2}\,\mu_B |g|\, B + \left(\frac{\pi}{8}\right)^{1/2} \frac{e^2}{\epsilon_L l}\,. \tag{26}$$

According to the last formula, the expected spin-energy gap for the filling factor $\nu = 1$ in a magnetic field of 8 T is $\Delta E_s = 2E_a \approx 190$ K, which significantly exceeds the measured values.

Similar data are also obtained applying other methods. For example, Fig. 18b shows the results of the measurement of the chemical potential jump using magneto-capacitive methods. Although the results presented in Figs 18a and b slightly differ quantitatively, they give the same scale of the energy gap and the same shape of its functional dependence on the magnetic field induction.

From Fig. 18b, one can make another important conclusion. Because the straight line drawn through the points in the inset to this figure corresponds, with a good accuracy, to the cyclotron mass, one can state that there is no exchange energy contribution to the spin splitting in the case of the filling factor $\nu = 2$. This is not surprising, because the corresponding contribution is proportional to the ratio [11]

$$\frac{n_\uparrow - n_\downarrow}{n_\uparrow + n_\downarrow}\,, \tag{27}$$

where $n_\uparrow$ and $n_\downarrow$ correspond to the filling of two spin sublevels of one Landau level.

Thus, it has been experimentally found beyond doubt that, owing to the electron–electron interaction, the spin energy gaps are much increased with respect to the Zeeman splitting. According to the theoretical expectations, the exchange increase of the spin spectral gap depends on the filling factor: it is maximum for odd filling factors, and vanishes for even ones.

The overall promising picture is disturbed by two facts. First, the functional dependence of the spin splitting on the magnetic field at odd filling factors contradicts the theoretical expectations. It turned out to be much closer to a linear function than to a square root one. A small deviation from the linear dependence was observed only in Ref. [74]. Second, the splitting is too small with respect to the expected one.

It was tempting to explain the 'incorrect' functional dependence by the influence of noncontrolled factors [75]. Indeed, there are plenty of such factors: the chaotic potential remaining in the two-dimensional electron system; the finite width of the electron wave function in the direction normal to the interface, and the inhomogeneity of the electron concentration. However, the reproducibility of the linear dependence in different samples and for different measurement methods makes such an assumption doubtful. Possibly, an important point missing in the theory is the fact that in the magnetic fields in which the measurements are performed the exchange energy of an ideal electron system equals or even exceeds the cyclotron energy.

Formally, equation (26) predicts the existence of a finite energy gap for the filling factor $\nu = 1$, even when the Landé factor $g = 0$. Under these conditions, complete spin polarization is impossible, and the above-considered pairs of an electron with a flipped spin projection and a vacancy cannot be the current-carrying excitations. The corresponding theoretical problem was considered in Ref. [76]. It is shown that in this case at a finite temperature charge-carrying pairs of spin structures emerge (one of which is schematically given in Fig. 19a), known as skyrmions and antiskyrmions. One should keep in mind that, although the picture in Fig. 19a looks similar to the lattice model, the spin structure is realized in the electron liquid and has an enhanced (for a skyrmion) or reduced (for an antiskyrmion) electron density; hence, every one of these structures carries a unit electric charge.

The activation energy of the skyrmion–antiskyrmion pair is half as big as the one defined by formula (26) at the zero Landé factor. The spatial size of the skyrmion decreases with an increase in the g-factor, and the activation energy increases

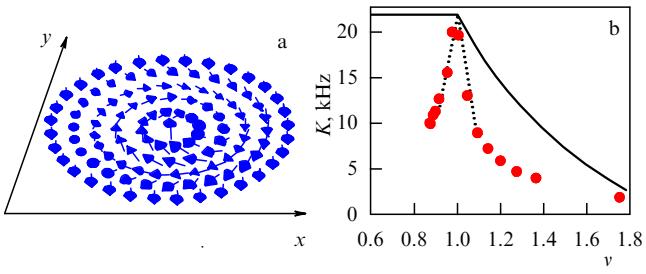

Figure 19. (a) Schematic image of a spin soliton, a skyrmion. (b) The Knight shift as a function of the filling factor (the electron density is fixed and the magnetic field is varied under the condition that the temperature dependence be saturated). The solid line corresponds to noninteracting electrons. The dotted line corresponds to the skyrmions (antiskyrmions) containing 3.6 electrons with flipped spin. (Data taken from Ref. [77].)

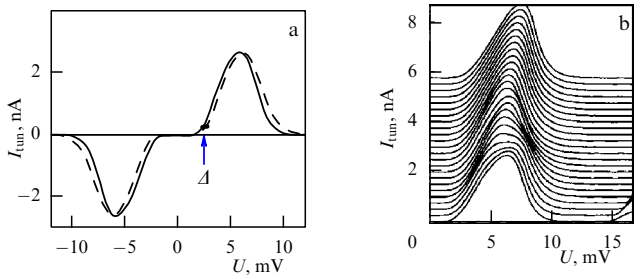

Figure 20. (a) Tunnel current I_{tun} as a function of voltage across the quantum wells at $B = 8$ T, and $T = 0.6$ K. The solid line corresponds to a sample with the barrier width 175 Å, and the dashed one to 340 Å. In the second case, the current values are increased by a factor of 3.6 for the convenience of comparison. (Data taken from Ref. [83].) (b) A series of curves corresponding to magnetic field variations from 8 T to 13 T. For convenience, the curves are shifted along the vertical direction. (Data taken from Ref. [82].)

with an increase in the Landé factor up to its some critical value g_c, above which skyrmions do not exist.

So far, there is no direct proof of the existence of skyrmions under the conditions of the quantum Hall effect. Most convincing indirect evidence is presented in Refs [77, 78], where the nuclear magnetic resonance was investigated in ^{71}Ga nuclei embedded in an $Al_{0.1}Ga_{0.9}As$ barrier bounding a GaAs quantum well with a high-mobility electron gas. The authors measured the frequency variation of the nuclear magnetic resonance caused by the influence of the spins in the electron system (the so-called Knight shift) depending on the filling factor in the vicinity of $\nu = 1$. The value of the shift K is determined by the degree of polarization of the electron system (Fig. 19b) equal to unity for integer filling and dropping dramatically on both sides of the value corresponding to the integer filling. The fit (dotted curve in Fig. 19b) of the theoretical dependence to the experimental data gives evidence that every spin-flipped electron also flips the spin of three electrons, which can be interpreted as the emergence of small-sized skyrmions, possibly embedded in the lattice [79].

5.3 Coulomb gap

Already in the early studies of tunneling into a two-dimensional electron system, it was discovered on measurements of samples of modest quality [80, 81] that the presence of a quantizing magnetic field decreases the tunneling probability. In these studies, tunneling into the two-dimensional electron gas occurred from a three-dimensional electrode, and the effect vanished with increasing the temperature.

A more impressive result was obtained in Refs [82, 83], which studied the tunneling between two identical quantum wells, each containing a high-mobility two-dimensional electron gas. The wells were separated by a tunnel-penetrated barrier whose width varied for different samples within a broad range from 175 to 340 Å.

Some of the experimental dependences obtained are shown in Fig. 20. As predicted, the tunnel current is antisymmetric depending on the voltage U across the quantum wells (Fig. 20a). Unexpected is the fact that the tunnel current was strongly suppressed within some interval $|U| < \Delta$ near the zero voltage. As one can see from Fig. 20b, the width of this interval increases as the magnetic field is strengthened. The effect is observed at filling factors both higher and lower than unity, but completely vanishes with increasing temperature or in a zero magnetic field.

In all the studies [80–84], the suppression of the tunnel current depended on the filling factor weakly and smoothly. Most probably, the reason for the tunnel current suppression is the presence of electrostatic interactions. Indeed, the charge spreading in the electron system placed in a quantizing magnetic field is slow and can be neglected during the tunneling. The escape of an electron from the electroneutral layer, as well as the embedding of an electron into an initially electroneutral layer, require the expenditure of additional energy, determining the scale of Δ.

The tunnel current suppression can be interpreted as the emergence of the Coulomb gap (sometimes called the pseudogap) in the tunnel density of states. Its weak dependence on the filling factor means that the gap is linked to the chemical potential level and shifts together with it. Theoretically, the Coulomb gap under quantum Hall effect conditions has been considered in a large number of publications within a broad range of filling factors corresponding to the metallic conductivity (see, for example, Refs [85–87]). The authors demonstrated that an exponentially small tunnel density of states can exist within the energy interval Δ which, however, significantly exceeds the one observed in the experiment. The most adequate theoretical description of the results obtained in Refs [80, 81] can be found in Ref. [88].

Exceptionally informative is Fig. 21 which, in particular, perfectly shows the Coulomb gap, as well as an increase in the spin gap in the vicinity of odd filling factors and spin-splitting oscillations. From Fig. 21 one can extract unique informa-

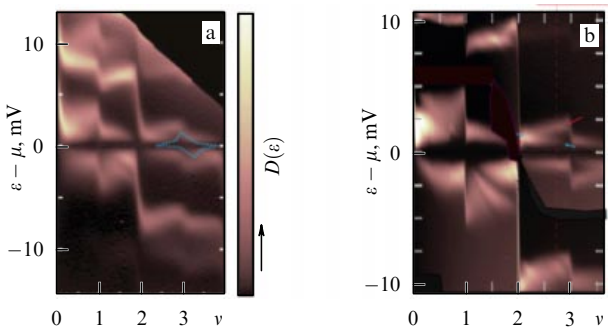

Figure 21. Tunnel density of states as a function of energy counted off from the chemical potential level and of filling factor in two samples of different quality in a magnetic field (a) $B = 4$ T, and (b) $B = 6$ T. (Data taken from Refs [89, 90].)

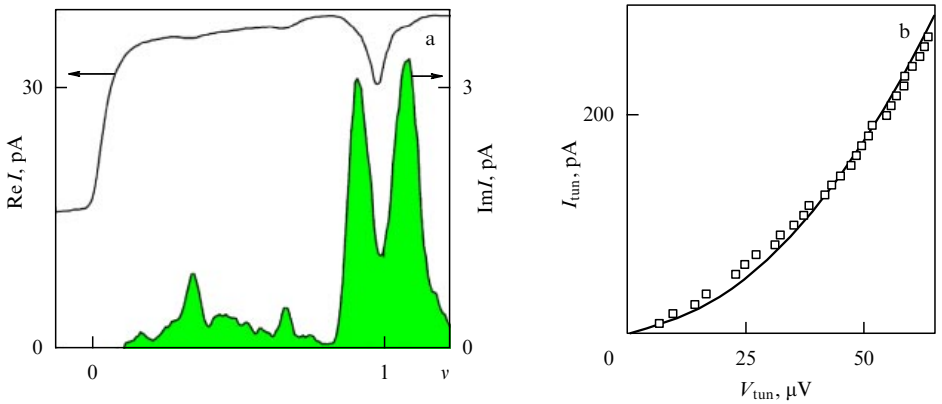

Figure 22. (a) Real and imaginary components of the current in the three-electrode structure similar to the one shown in Fig. 8, as a function of filling factor at $T = 30$ mK, $B = 14$ T, $U = 4.2$ mV, and $\omega/2\pi = 73$ Hz. (b) The experimental values (squares) and the fit (solid curve) from Eqns (28), (29) of the volt–ampere characteristic at $B = 13$ T and $T = 60$ mK. (Data taken from Ref. [92].)

tion, although without its theoretical explanation: the Coulomb gap replicas, expected only on the Fermi level, can also be observed at empty and fully filled quantum levels.

A Coulomb gap of another origin was discovered while investigating a three-electrode system similar to the system shown in the inset to Fig. 8 [91, 92]. One of the pairs of original experimental curves analyzed in Refs [91, 92] are plotted in Fig. 22a. One should notice that the real component of the current flowing through the structure depends on both the capacity and the tunnel resistance. A significant real part exists, according to Refs [80–83], at all investigated filling factors; however, in the vicinity of the filling factor $\nu = 1$, where the sample is found in an insulating state, it is increased. The real component of the current has a double-humped shape, which is related to the dip in the capacity. The effect shows a strong dependence on the filling factor, and it has not been observed for other integer filling factors.

From two known components of the current flowing through the structure one can calculate both the tunnel current and the voltage drop on the tunnel barrier. The corresponding dependence is displayed in Fig. 22b. As one can see, this dependence is close to parabolic.

According to the theory [93, 94], the tunnel density of states $D(\varepsilon)$ under the conditions considered here has the form

$$D(\varepsilon) = D_\mu + \alpha|\varepsilon - \mu|\,, \tag{28}$$

which leads to the following dependence of the tunnel current on voltage:

$$I_{\rm tun} = \gamma \int_{-\infty}^{\infty} D_{\rm m} D(\varepsilon) \left[f(\varepsilon - eV_{\rm tun}, T) - f(\varepsilon, T) \right] {\rm d}\varepsilon\,. \tag{29}$$

Here, $D_{\rm m}$ is the density of states in an electrode made of a three-dimensional metal, and $f(\varepsilon, T)$ is the Fermi–Dirac distribution function. A fit of relations (28), (29) at $D_{\rm m} = {\rm const}$, using a single fitting parameter $D_{\rm m}\alpha\gamma$, shown in Fig. 22b by the solid line, sufficiently well describes the experimental results.

5.4 Stripe phases

Yet another effect caused by the interactions between electrons has been discovered in the two-dimensional electron structures of a record-high quality with a mobility of around 10^7 cm^2 V^{-1} s^{-1}. In such structures, the unusual

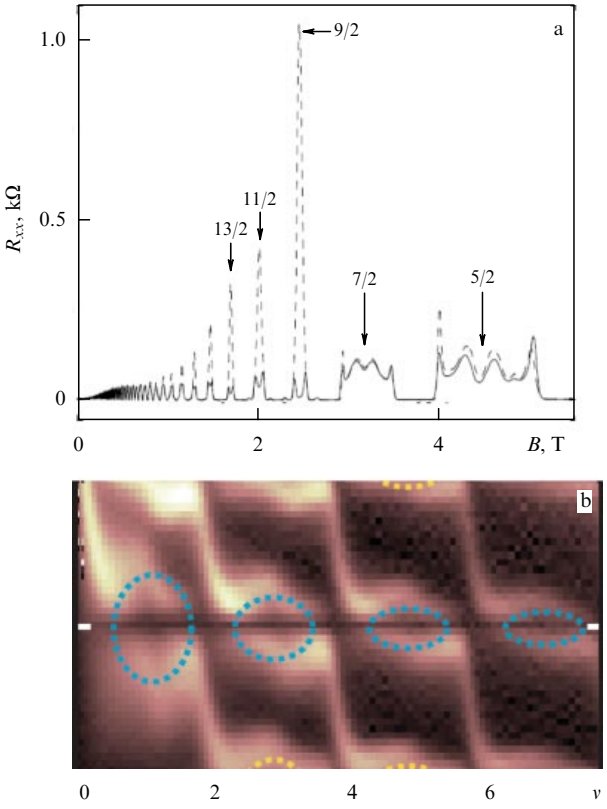

Figure 23. (a) Dependence of the resistance on magnetic field in a heterostructure with the mobility 9×10^6 cm^2 V^{-1} s^{-1} at the temperature 25 mK. Two records (solid and dashed lines) correspond to orthogonal current directions. (Data taken from Ref. [95].) (b) The tunnel density of states in the field $B = 2$ T. For every investigated filling factor, the Coulomb gap is clearly visible on the chemical potential level. (Data taken from Ref. [90].)

behavior of R_{xx} was observed in the vicinity of its maxima at filling factors $\nu = M + 1/2 \geqslant 5/2$. An example of the experimental record from Ref. [95] is given in Fig. 23a. As one can see from the figure, either a complicated structure or a growing peak of the conductivity is observed at low temperatures, $T \leqslant 150$ mK, at the maxima of the dissipative resistance as the temperature decreases. At filling factors exceeding 7/2, the result depends on the direction of the current: at the current flowing along the crystallographic

direction [110], the resistance is relatively small ($\approx 50\ \Omega$), and a much higher peak in the resistance ($\approx 1000\ \Omega$) is observed for the orthogonal direction. These features of the dissipative resistance are not followed by additional plateaus emerging in the Hall component. A similar structure is also observed in the vicinity of the maxima of R_{xx} at filling factors 5/2 and 7/2, but in this case there is no anisotropy of the resistance dissipative component.

The theoretical considerations explaining the discovered effect appeared even before the experiment was performed (see Refs [96, 97]). For $M \gg 1$, a homogeneous system with a half-integer filling factor $\nu = M + 1/2$ turns out to be energetically unfavorable; therefore, the upper filled quantum energy level in one part of the sample plane gains the filling factor $\nu = M + 1$, and in the other $\nu = M$. The shape and the size of areas with different filling factors are determined by the competition between the exchange interaction, which lowers the energy of the ground state of the electron system as the integer filling takes place, and the Coulomb energy. For an average filling factor $\nu = M + 1/2$, the optimal configuration in the Hartree–Fock approximation turns out to be a system of parallel stripes with a characteristic width on the order of the cyclotron radius. The electron system spontaneously breaks down its symmetry with the formation of the charge-density wave. However, if the filling factor is not closer to a half-integer value but to an integer one, then it is possible that an isotropic inhomogeneous phase emerges from separate islands forming something similar to a crystal. Finally, the emergence of a Wigner crystal is theoretically predicted in the vicinity of an integer filling factor — that is, the spontaneous appearance of a strong modulation of the electron density with the maxima forming a regular (presumably triangular) lattice, and almost a 100% probability of detecting an electron in the vicinity of each maximum.

Such a picture agrees with the anisotropy of the dissipative component of the resistivity tensor. It is interesting to note that, within the framework of this picture, the existence of the Coulomb gap is also predicted in the case of tunneling to the chemical potential level at high filling factors. The gap originates from the exchange interaction, and in the case of half-integer filling its width equals

$$\Delta E_{\mathrm{g}} = \frac{r_{\mathrm{s}}\hbar\omega_{\mathrm{c}}}{\sqrt{2\pi}} \ln\left(1 + \frac{0.3}{r_{\mathrm{s}}}\right) + \hbar\omega_{\mathrm{c}} \frac{\ln\left(Mr_{\mathrm{s}}\right)}{2M+1}\,. \qquad (30)$$

At a fixed filling factor, the second term on the right-hand side of formula (30) is proportional to the magnetic field. The gap is well pronounced in the tunnel spectra taken in Ref. [90] (Fig. 23b), although its field dependences have not been properly studied yet.

The Hartree–Fock approximation gives only a rough description of the situation. In the series of studies [98–101], the spatial distribution of the areas with different filling factors was considered in terms that are traditionally used for the description of liquid crystals, and on going beyond the Hartree–Fock approximation an even greater abundance of realizable phases has been discovered. For example, the above-considered structure of collinear stripes can be treated as a smectic, but if the stripes are not strictly parallel and the stripe structure contains disorder with the conservation of the primary direction, then such a phase corresponds to a nematic. The rupture of stripes is possible with the formation of a stripe crystal, etc.

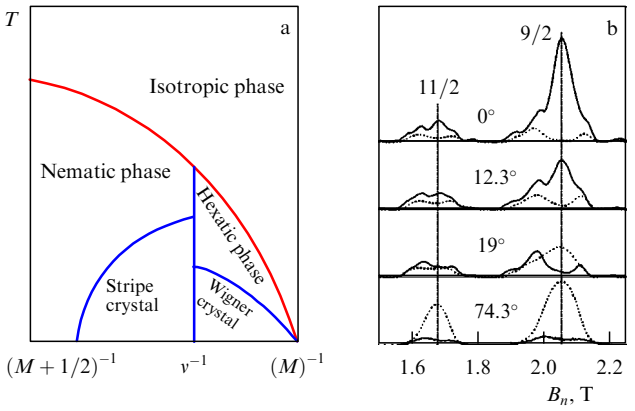

Figure 24. (a) Phase diagram for the ground state of stripe phases at a finite temperature. (Data taken from Ref. [96].) (b) The influence of the magnetic field tilt on the dissipative component R_{dis} of the resistance. The magnetic field is tilted with respect to the normal in the direction parallel to the initial orientation of the stripes. The dotted line corresponds to the current flowing along the [110] axis, and the solid line is the current flowing in the perpendicular direction. (Data taken from Ref. [102].)

A version of the phase diagram, proposed in Ref. [96], is illustrated in Fig. 24a. As the temperature decreases, an ordinary isotropic liquid, depending on the filling factor, is replaced either by nematic stripes or by a hexatic (the intermediate phase between a crystal formed by islands and the disordered distribution of the same islands). A further temperature decrease leads to the formation of either a Wigner crystal or a stripe crystal, and only in the vicinity of a half-integer filling factor does the nematic phase remain.

Unfortunately, the experimental feasibilities for exploring the stripe phases are strongly limited. So far there are no methods that allow a detailed investigation of the spatial structure of the phases. The main information was obtained from the study of electroresistance anisotropy. It was discovered (see Fig. 24b) that the emergence of the magnetic field component that is primarily parallel to the initial orientation of the stripes changes the anisotropy — that is, changes their orientation. By introducing a magnetic field component orthogonal to the stripe orientation, one can stabilize the initial anisotropy. Finally, for filling factors 5/2 and 7/2, anisotropy can be achieved by tilting the magnetic field [102]. Passing of a direct current on the order of 1 μA can also influence the anisotropy and the stability boundaries of different phases [103].

In the smectic phase, the passing of a current should cause the drift of a charge-density wave in the direction perpendicular to the orientation of the stripes and lead to nonstationary effects. Conceivably, it has been the drift of the charge-density wave that was observed in Ref. [104], although no link between the noise detected in this work and the motion of the stripe phase has been reliably demonstrated.

6. Integer quantum Hall effect in exotic two-dimensional electron systems

6.1 Graphene

The best known and most popular exotic two-dimensional electron system is, undoubtedly, graphene, recently introduced into research [105]. This material constitutes a monolayer of graphite (Fig. 25a) with a crystal lattice that

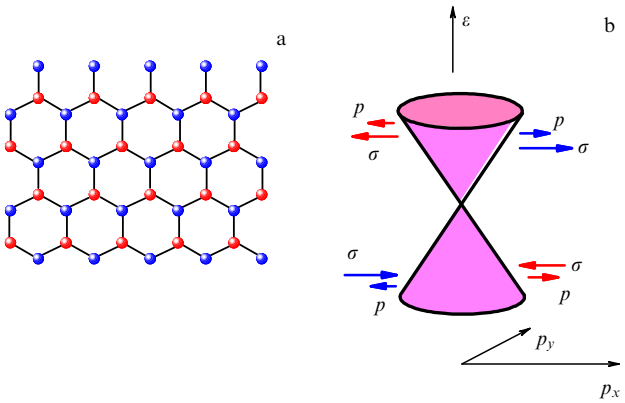

Figure 25. (Color online.) (a) Schematic of a graphene crystal lattice. Different colors visualize two equivalent triangular sublattices. (b) The graphene energy spectrum (one of two valleys); σ is the pseudospin projection.

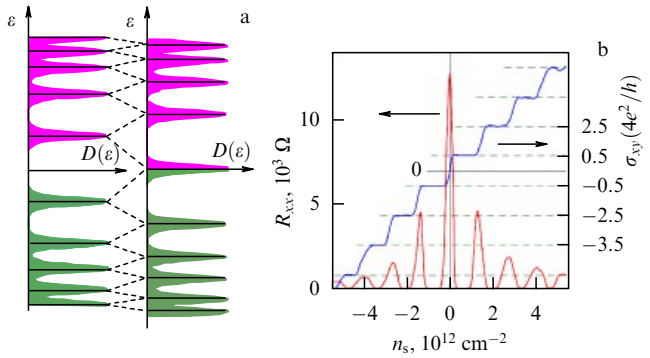

Figure 26. (Color online.) (a) Schematic picture of the density of states as a function of energy (the left-hand side of the figure corresponds to Eqn (32), the right one corresponds to Eqn (33). The electron and hole quantum levels are shown in different colors. (b) The experimental results for the Hall conductance component and the dissipative component of the magnetoresistance tensor in graphene at $B = 14$ T and $T = 4$ K. (Data taken from Ref. [106].)

can be represented as two triangular sublattices. In a free state, the monolayer folds into a roll; therefore, one should deposit it on a dielectric substrate (for example, SiO_2), which allows one to make a field-effect transistor based on graphene, and to control the electron density in the monolayer. Most experiments were performed using graphene with a substrate made of oxidized silicon.

Initially, special attention to graphene was due to its electron spectrum having the shape of two cones with a single common point (Fig. 25b). It is important for us that the spectrum greatly differ from a parabolic one and, hence, in the magnetic field the quantum levels, unlike those given by formula (4), are not equidistant. Another distinctive feature of the graphene electron spectrum is related to the presence of two equivalent crystal sublattices. In a fixed momentum direction, the electron wave function can be represented as a linear combination of the wave functions related to one of the sublattices. Such a situation is usually described using an additional quantum number (pseudospin σ).

At the boundary of the first Brillouin zone, graphene has two sets of points where $\varepsilon(\mathbf{p}) = 0$. In the extended-zone scheme, there are two valleys with a dispersion relation that corresponds to the energy spectrum schematically illustrated in Fig. 25b.

In the case of a nonparabolic electron spectrum, it is convenient to begin with the quasiclassical Bohr–Sommerfeld quantization condition in defining the quantum level system in a magnetic field, which requires [22] the quantization of the electron orbit area in the momentum space to satisfy the following relation

$$S_n = \left(n + \frac{1}{2}\right)\frac{heB}{c}\,. \tag{31}$$

Applying relationship (31) to the graphene electron spectrum $\varepsilon(\mathbf{p}) = \pm c^*|\mathbf{p}|$, we obtain

$$\varepsilon_n = \pm\left[\left(n + \frac{1}{2}\right)\frac{heBc^{*2}}{\pi c}\right]^{1/2}. \tag{32}$$

Here, the plus sign is related to the electron quantum levels, and the minus sign is related to the hole levels. The corresponding spectrum is displayed on the left-hand side of Fig. 26a. This is how the spectrum looks if we neglect valley and spin splittings. However, the valley splitting in graphene is comparable to the cyclotron one (see, for example, Ref. [107]), and spectrum (32) has the form

$$\varepsilon_n = \pm\left[\left(n + \frac{1}{2} \pm \frac{1}{2}\right)\frac{heBc^{*2}}{\pi c}\right]^{1/2}, \tag{33}$$

which corresponds to the right-hand side of Fig. 26a. The quantum levels are four-fold degenerate (twice in the spin index, and twice in the valley one). Each of them is composed of two neighboring Landau levels. One of the quantum levels, corresponding to zero energy, consists of a quantum sublevel for the electrons and of the same sublevel for the holes. Therefore, the quantization condition takes on the form

$$n_s = \pm 4n_0\left(N + \frac{1}{2}\right). \tag{34}$$

As one can see from Fig. 26b, the experimental curves agree with equation (34).

The spin splitting of the levels, which we have been neglecting up to this point, can significantly change the dependences of the Hall and dissipative conductivities near the point where the charge-carrier density turns to zero. An additional plateau $\sigma_{xy} = 0$ emerges in the vicinity of this point at a finite value of the dissipative conductance [108]. Another specific feature of the graphene electron spectrum in a quantizing magnetic field is the large energy gap between the quantum levels with the smallest numbers. It was utilized in Ref. [109], where an integer quantum Hall effect was observed at room temperature ($T = 300$ K) in a magnetic field of 29 T.

6.2 Two-dimensional semimetal

This section and next Section 6.3 are based on the results of research into electron gas in quantum wells of one type (HgTe in HgCdTe with the surface orientation (013)), but with different widths. Let us begin by considering wide quantum wells with a width of about 18–21 nm (Fig. 27a). The electron spectrum in such a quantum well has the typical semimetal behavior,[3] which is shown schematically for the $[0\bar{3}1]$ direction in Fig. 27c. There is an electron minimum in the

[3] The semimetal character of the two-dimensional electron spectrum can also be realized in wide quantum wells produced from the same material with a surface orientation (112) or (100).

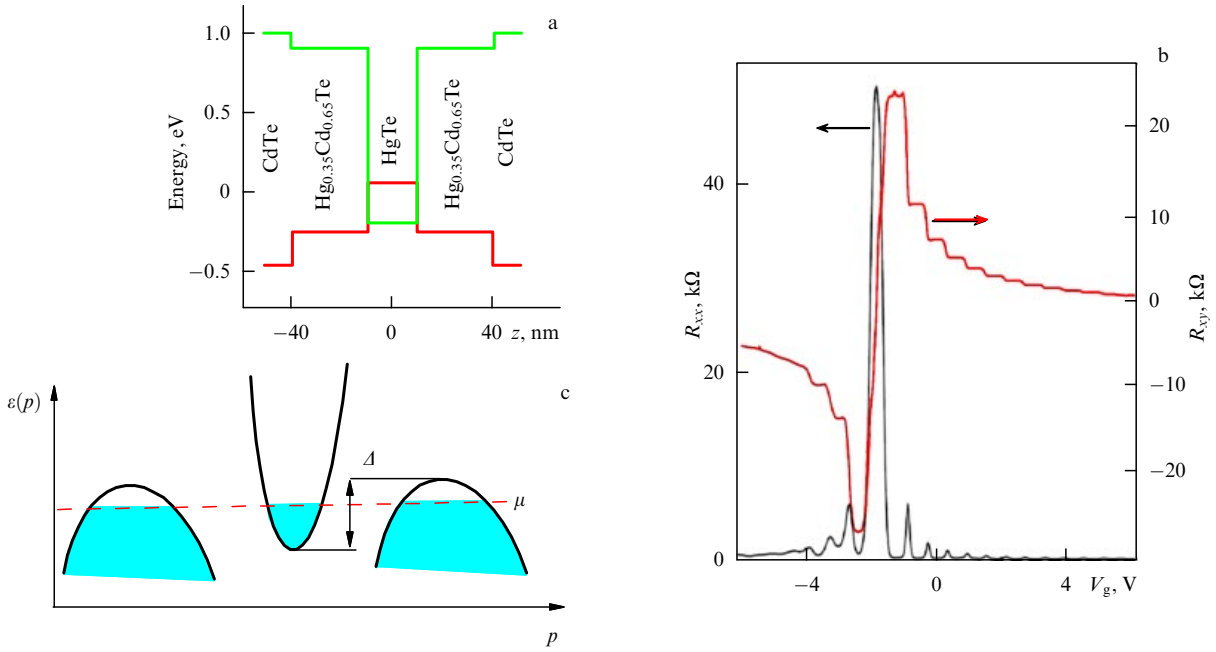

Figure 27. (a) Dependence of the conduction band bottom and the valence band top on the depth in a wide HgTe quantum well in HgCdTe. (b) The experimental plots of the dissipative and the Hall components of the magnetoresistance tensor versus the gate voltage at $B = 2$ T, and $T = 0.19$ K. In a zero magnetic field, the charge electroneutrality point corresponds to the gate voltage $V_g = -1.2$ V. (c) The schematic pattern of the electron spectrum.

center of a two-dimensional Brillouin zone (related to the minimum of the heavy-holes first zone (h1) at the point Γ) and two hole maxima (related to the maxima of the heavy-holes second zone (h2)) that are shifted in the k-space along the $[0\bar{3}1]$ axis at a distance of the order of 0.3 nm^{-1} with respect to the midpoint of the Brillouin zone. The experimental values for the density of states masses are $m_h \approx 0.15m_0$, $m_e \approx 0.025m_0$, where m_0 is the free electron mass [110, 111].

As in three-dimensional semimetals, there is an energy region Δ where the electron and hole bands overlap, and both the electrons and holes are present in the two-dimensional system, as long as the chemical potential is located within this region. Their densities are equated at the point of charge electroneutrality for the concentration $n_{e0} = p_{h0} \approx 5 \times 10^{10}$ cm^{-2}. The overlap energy and the chemical potential at the electroneutrality point are determined by the effective masses and the concentration of the charge carriers. Counting off all the energies from the bottom of the conduction band, we obtain

$$n_{e0} = p_{h0} = \frac{\mu_0 g_{se} m_e}{2\pi\hbar^2} = \frac{(\Delta - \mu_0) g_{sh} g_{vh} m_h}{2\pi\hbar^2}, \qquad (35)$$

where g_s and g_v are the degrees of the spin and valley degeneracies, respectively. Let us point out that the gate voltage does not determine the electron and hole concentrations, but their difference, while the values proper of the concentration, according to expression (33), are determined by the electron spectrum.

In a quantizing magnetic field, the upper partly filled electron quantum level and the lowest partly filled hole quantum level do not generally coincide in energy. Such a situation is impossible in the equilibrium state, and electron–hole recombination takes place, until at least one of the partly filled quantum levels becomes completely empty. During this process, the chemical potential is oscillating, becoming either pinned to the partly filled quantum level or located in the midpoint between the fully filled level and the nearest empty one. The electron–hole recombination has no influence on the spectrum, because the quantum well, at least in the roughest approximation, is hard [112]. The quantization conditions for a nondegenerate spectrum are similar to those that are valid for graphene:

$$n_s = \pm n_0 N. \qquad (36)$$

As one can see from Fig. 27b, condition (36) is fully confirmed by experiment, and every quantum level turns out to be non-degenerate. Such a picture is in quite good agreement with the result of electron spectrum calculations [113], which turns out to depend on the magnetic field value and to be significantly different from ordinary intersecting Landau fans. The complicated behavior of the spectrum is related to the strong spin–orbit interaction in the medium under consideration. However, the peculiarities of the spectrum are barely pronounced in the fan diagrams similar to the ones shown in Fig. 10b, which are plotted using the experimental results.

Despite the similarity of Figs 26b and 27b, there is a significant difference between graphene and the two-dimensional semimetal: the chemical potential level coincides with the quantum level at the charge-electroneutrality point of the graphene (with an accuracy up to the spin splitting), and in the two-dimensional semimetal it is located in the energy gap. The number of electrons and holes at the charge-electroneutrality point are not fixed and vary from the value which is typical in a zero magnetic field to zero in the strong field. Therefore, $\rho_{xy} = 0$ in the latter case, and ρ_{xx} has an activation behavior [114] with an unexpectedly small value of activation energy that indicates the complexity of the electron spectrum [113].

6.3 Quantum spin Hall insulator

Let us proceed now to the consideration of the properties of the same quantum well, as in Section 6.2, but with a significantly smaller width. As the width of the quantum well decreases, first, the overlap of the heavy-hole zones disappears, and then at the critical well width of 6.3 nm zones e1 and h1 intersect at the point Γ of the Brillouin zone. The zone intersection is related to the influence of HgCdTe, which surrounds the quantum well and exhibits a sequence of atomic zones that is different from the one in HgTe. Zone e1 itself contains two spin states of the atomic s-orbitals, while zone h1 is formed from the p-orbitals with the spin projection of $\pm 3/2$.

Let us turn to an electron spectrum in some vicinity of the point Γ for the case of the well width close to the critical one. Far from the edge of the two-dimensional electron system, the spectrum should be described in terms of the Hamiltonian which takes into account the mixing of zones e1 and h1, because of the strong spin–orbit interaction that is related to the presence of p-orbitals. At the critical well width, the electron spectrum is similar to the graphene spectrum, except for the fact that it has one valley, because in the spectrum considered the zones intersect at the point Γ. For well widths both smaller (the noninverted spectrum) and larger (the inverted spectrum) than the critical one, there is an energy gap in the strongly nonparabolic spectrum. In the case of a spectrum noninverted at the point Γ, the wave functions in the conduction band are constructed from the s-orbitals, and in the valence band from the p-orbitals, and the way they are constructed does not change with an increase in the wave vector value. Vice versa, for the spectrum inverted at the point Γ the wave functions in the conduction band are constructed from the p-orbitals, and in the valence band from the s-orbitals, and the way they are constructed changes with an increase in the wave vector value. It is clear that by placing the chemical potential level within the energy gap, we will have to do with an insulator in both considered cases, but these insulators would be topologically nonequivalent. If the first of them (the one with the noninverted spectrum) is well known as an ordinary two-dimensional insulator, the properties of the second one (the two-dimensional topological insulator) should be discussed in detail, because it demonstrates the effect known as the quantum spin Hall effect.

The quantum spin Hall effect shows itself as the existence of discrete conductance related to the emergence of spin-polarized electrons on the side boundaries even in the absence of a magnetic field.

Let us proceed to the consideration of a spatially limited two-dimensional electron gas. For definiteness, let us place the boundary at $x = 0$, so the gas occupies the half-plane with $x \geqslant 0$. For the noninverted spectrum behavior, the breaking of the translational symmetry along the x-axis does not itself cause the emergence of the additional quantum states in the bulk spectral gap. The situation is different for the inverted spectrum. The absence of translational symmetry leads to a necessity of changing the mixing of the zones e1 and h1 near the boundary of the two-dimensional electron gas. As a result, a one-dimensional gapless state emerges at the boundary with the wave function being zero at $x = 0$, and with an amplitude that is described by the sum of two exponents.

This kind of state can emerge only in the vicinity of the point Γ in the Brillouin zone, where at $k = 0$ it is four-fold degenerate: twice in the spin projection, and twice in the atomic zones combination. We are interested in the dependence of the edge-state energy on the momentum component k_y that remains a good quantum number near the boundary.

The one-dimensional Hamiltonian describing the dependence of interest assumes the form [115]

$$H_{\text{edge}} = Ak_y\sigma^z . \tag{37}$$

For an HgTe quantum well, the parameter $A = 0.36$ eV, and the velocity $v = A/\hbar = 5.5 \times 10^7$ cm s^{-1}. Already from the form of the Hamiltonian one can see that the group velocity of the electrons with positive spin projections does not depend on their energy and has an opposite sign with respect to the group velocity of the electrons with the opposite spin projections. The edge state has a one-dimensional graphene-like spectrum. The direction of path tracing along the sample boundary (clockwise or counter-clockwise) is controlled by the parameters of the initial bulk Hamiltonian, and in equation (37) by the sign of parameter A.

Thus, by fixing the chemical potential level in the gap of the bulk spectrum, we will intersect it near every edge by two one-dimensional edge channels that transport the electrons in opposite directions and with opposite spin projections.

If the sample has a rectangular shape and an ohmic contacts, the situation is even more similar to the one under the integer quantum Hall effect conditions. Let us assume that at the beginning we have only two contacts: the emitter, and the collector with different chemical potentials. On every side connecting the contacts of the sample, the charge and the spin transfers appear. But the chemical potential levels for the spin 'up' ('down') will be different on different sides: therefore, a nonequilibrium spin population, proportional to the current, will emerge. At the same time, the electric currents flowing along the opposite sides of the sample have the same values and directions. The two-contact conductance of the sample, calculated using the Büttiker formalism (see Section 3.4), equals $2e^2/h$.

More interesting is the situation when the sample also possesses potential contacts. In this case, both the two-contact resistance and the potential difference between the contacts depend on the number and on the location of the potential contacts. For example, if there is only one pair of such contacts on every side, then the drop of potential, measured between the two neighboring contacts, corresponds to the resistance $h/2e^2$, and the two-contact resistance between the collector and the emitter equals $3h/2e^2$. The given values are easily calculated using the Büttiker formalism as well.

The expected picture of the edge states has some similarity with the one in the case of the integer quantum Hall effect, which was the reason for introducing the term 'quantum spin Hall insulator'.

One has to point out that the above discussion is valid only in the absence of electron back scattering, related to spin flip. At low temperatures and in the absence of magnetic impurities, such processes are assumed to have a small probability.

In the experiment [116] (Fig. 28), the resistance behavior similar to the predicted one (see above) was indeed observed. For two potential contacts on every side of the rectangular sample, the resistance between the contacts of one side indeed was $h/2e^2$, not depending on the sample width. Such a resistance value was only observed in the quantum well with the inverted spectrum. Surprisingly, it turned out that for the

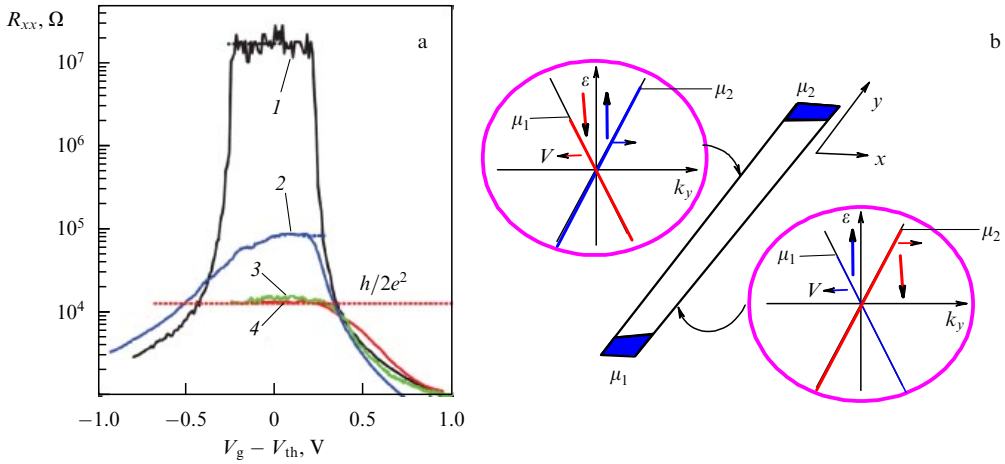

Figure 28. (a) Results of measurements performed in Ref. [116]: *1* is for a quantum well with the noninverted spectrum, and *2–4* are for quantum wells with the inverted spectrum. In cases *1* and *2*, the length of the samples is 20 μm, and in cases *3* and *4* the sample length is 1 μm, but the width of one of them is twice the width of the other one; $T = 30$ mK. (b) A schematic picture of the sample for the two-contact measurements, $\mu_1 < \mu_2$. In the insets, the edge channel spectra and their filling on the opposite boundaries of the sample are presented; the horizontal arrows indicate the direction of the electron velocity, and the vertical ones show the spin z-projection.

observation one needs very short samples, with a length on the order of 1 μm. The reason for the frequent scattering processes that take place between the one-dimensional channels remains unknown.

When applying a quantizing magnetic field to the two-dimensional electron system in the state of the quantum spin Hall insulator, such a state must be destroyed because the initial symmetry of the edge channels differs from the edge channel symmetry in the state of the integer quantum Hall effect. Experiment [116] confirms this inference.

7. Conclusion

Let us formulate the unsolved problems and outline possible avenues for further research in the field of the integer quantum Hall effect.

(1) The determination of the theoretical limit of the reproducible-digits number in the quantum Hall effect.

(2) The resolution of the conflict between the theory and the experiment, related to the functional dependence of the spin gap on the magnetic field at the fixed filling factor.

(3) The explanation of the existence of the Coulomb gap replicas on the quantum levels above and below the chemical potential level.

(4) The visualization of the stripe phases structure.

(5) The investigation of the quantum Hall effect in exotic two-dimensional electron systems.

Of course, the above-introduced list represents the tastes and interests of the author and is not universal, although it can turn out to be useful as a reminder of the imperfection of our knowledge in this field.

Acknowledgments

The author is sincerely grateful to I S Burmistrov, V F Gantmakher, E V Devyatov, Z D Kvon, V S Khrapai, and A A Shashkin for the fruitful discussions. This work was financially supported by the Russian Academy of Sciences, the Ministry of Education and Science of the Russian Federation, and the Russian Foundation for Basic Research. The author is grateful to the Dmitry Zimin Dynasty Foundation for the opportunity to give a lecture on the review topic at the Summer School 2013, 'Topical Problems in Condensed State Physics (Theory and Experiment)'.

References

1. Klitzing K v, Dorda G, Pepper M *Phys. Rev. Lett.* **45** 494 (1980)
2. Rashba E I, Timofeev V B *Sov. Phys. Semicond.* **20** 617 (1986); *Fiz. Tekh. Poluprovod.* **20** 977 (1986)
3. Huckestein B *Rev. Mod. Phys.* **67** 357 (1995)
4. Das Sarma S, Pinczuk A (Eds) *Perspectives in Quantum Hall Effects* (New York: Wiley, 1997)
5. Mohr P J, Taylor B N *Rev. Mod. Phys.* **72** 351 (2000)
6. Devyatov E V *Phys. Usp.* **50** 197 (2007); *Usp. Fiz. Nauk* **177** 207 (2007)
7. Prange R E, Girvin S M (Eds) *The Quantum Hall Effect* (New York: Springer-Verlag, 1987)
8. Butcher P, March N H, Tosi M P (Eds) *Physics of Low-Dimensional Semiconductor Structures* (New York: Plenum Press, 1993)
9. Demikhovskii V Ya, Vugalter G A *Fizika Kvantovykh Nizkorazmernykh Struktur* (Physics of Quantum Low-Dimensional Structures) (Moscow: Logos, 2000)
10. Gantmakher V F *Electrons and Disorder in Solids* (Oxford: Clarendon Press, 2005); *Elektrony v Neuporyadochenykh Sredakh* (Electrons in Disordered Media) (Moscow: Fizmatlit, 2005)
11. Ando T, Fowler A B, Stern F *Rev. Mod. Phys.* **54** 437 (1982)
12. Laughlin R B *Phys. Rev. B* **23** 5633 (1981)
13. Landau L D, Lifshitz E M *Quantum Mechanics: Non-Relativistic Theory* (Oxford: Pergamon Press, 1977); Translated from Russian: *Kvantovaya Mekhanika: Nerelyativistskaya Teoriya* (Moscow: Fizmatlit, 2002)
14. Thouless D J *Phys. Rev. Lett.* **71** 1879 (1993)
15. Halperin B I *Phys. Rev. B* **25** 2185 (1982)
16. Büttiker M *Phys. Rev. B* **38** 9375 (1988)
17. Kent A J et al. *Phys. Rev. Lett.* **69** 1684 (1992)
18. Roshko S, Dietsche W, Challis L J *Phys. Rev. Lett.* **80** 3835 (1998)
19. Pines D, Nozières P *The Theory of Quantum Liquids* (New York: W.A. Benjamin, 1966)
20. Chklovskii D B, Shklovskii B I, Glazman L I *Phys. Rev. B* **46** 4026 (1992)
21. Wei Y Y et al. *Phys. Rev. Lett.* **81** 1674 (1998)
22. Abrikosov A A *Fundamentals of the Theory of Metals* (Amsterdam: North-Holland, 1988); Translated from Russian: *Osnovy Teorii Metallov* (Moscow: Nauka, 1987)
23. Dolgopolov V T et al. *Phys. Rev. B* **46** 12560 (1992)
24. Dolgopolov V T et al. *Phys. Rev. Lett.* **79** 729 (1997)

25. Baskin E M, Magarill L N, Entin M V *Sov. Phys. JETP* **48** 365 (1978); *Zh. Eksp. Teor. Fiz.* **75** 723 (1978)
26. Ando T, Aoki H *J. Phys. Soc. Jpn.* **54** 2238 (1985)
27. Shashkin A A, Dolgopolov V T, Kravchenko G V *Phys. Rev. B* **49** 14486 (1994)
28. Khmelnitskii D E *Phys. Lett. A* **106** 182 (1984)
29. Abrahams E et al. *Phys. Rev. Lett.* **42** 673 (1979)
30. Levine H, Libby S B, Pruisken A M M *Phys. Rev. Lett.* **51** 1915 (1983)
31. Shashkin A A, Kravchenko G V, Dolgopolov V T *JETP Lett.* **58** 220 (1993); *Pis'ma Zh. Eksp. Teor. Fiz.* **58** 215 (1993)
32. Glozman I, Johnson C E, Jiang H W *Phys. Rev. Lett.* **74** 594 (1995)
33. Gusev G M et al. *Solid State Commun.* **100** 269 (1996)
34. Dultz S C, Jiang H W, Schaff W J *Phys. Rev. B* **58** R7532 (1998)
35. Khmel'nitskii D E *JETP Lett.* **38** 552 (1983); *Pis'ma Zh. Eksp. Teor. Fiz.* **38** 454 (1983)
36. Wang C et al. *Phys. Rev. B* **89** 045314 (2014); arXiv:1307.7532
37. Pruisken A M M *Nucl. Phys. B* **235** 277 (1984)
38. Pruisken A M M *Phys. Rev. B* **32** 2636 (1985)
39. Dolgopolov V T et al. *Sov. Phys. JETP* **72** 113 (1991); *Zh. Eksp. Teor. Fiz.* **99** 201 (1991)
40. Pruisken A M M, Baranov M A *Europhys. Lett.* **31** 543 (1995)
41. Wei H P, Tsui D C, Pruisken A M M *Phys. Rev. B* **33** 1488 (1986)
42. Kawaji S, Wakabayashi J *J. Phys. Soc. Jpn.* **56** 21 (1987)
43. Wei H P et al., in *High Magnetic Fields in Semiconductor Physics. Proc. of the Intern. Conf., Würzburg, Fed. Rep. of Germany, August 18–22, 1986* (Springer Series in Solid-State Sciences, No. 71, Ed. G Landwehr) (Berlin: Springer-Verlag, 1987) p. 11
44. Shahar D et al. *Phys. Rev. Lett.* **79** 479 (1997)
45. Dolan B P *Nucl. Phys. B* **554** 487 (1999); cond-mat/9809294
46. Kravchenko S V, Perenboom J A A J, Pudalov V M *Phys. Rev. B* **44** 13513 (1991)
47. Dolgopolov V T et al. *JETP Lett.* **55** 733 (1992); *Pis'ma Zh. Eksp. Teor. Fiz.* **55** 701 (1992)
48. Murzin S S et al. *Phys. Rev. B* **66** 233314 (2002)
49. Xue Y, Prodan E *Phys. Rev. B* **87** 115141 (2013)
50. Koch S et al. *Phys. Rev. B* **46** 1596 (1992)
51. Wei H P et al. *Phys. Rev. B* **45** 3926 (1992)
52. Mil'nikov G V, Sokolov I M *JETP Lett.* **48** 536 (1988); *Pis'ma Zh. Eksp. Teor. Fiz.* **48** 494 (1988)
53. Huckestein B, Kramer B *Phys. Rev. Lett.* **64** 1437 (1990)
54. Evers F, Mirlin A D *Rev. Mod. Phys.* **80** 1355 (2008)
55. Shashkin A A *Phys. Usp.* **48** 129 (2005); *Usp. Fiz. Nauk* **175** 139 (2005)
56. Balaban N Q, Meirav U, Bar-Joseph I *Phys. Rev. Lett.* **81** 4967 (1998)
57. Iordansky S V *Solid State Commun.* **43** 1 (1982)
58. MacDonald A H, Rice T M, Brinkman W F *Phys. Rev. B* **28** 3648 (1983)
59. Shklovskii B I, Efros A L *JETP Lett.* **44** 669 (1986); *Pis'ma Zh. Eksp. Teor. Fiz.* **44** 520 (1986)
60. Dolgopolov V T et al. *Phys. Low-Dimens. Struct.* (6) 1 (1996)
61. Gavrilov M G, Kukushkin I V *JETP Lett.* **43** 103 (1986); *Pis'ma Zh. Eksp. Teor. Fiz.* **43** 79 (1986)
62. Mosser V et al. *Solid State Commun.* **58** 5 (1986)
63. Kukushkin I V, Meshkov S V, Timofeev V B *Sov. Phys. Usp.* **31** 511 (1988); *Usp. Fiz. Nauk* **155** 219 (1988)
64. Dorozhkin S I, Dorokhova M O *JETP Lett.* **71** 417 (2000); *Pis'ma Zh. Eksp. Teor. Fiz.* **71** 606 (2000)
65. Efros A L *Phys. Rev. B* **45** 11354 (1992)
66. Eisenstein J P, Pfeiffer L N, West K W *Phys. Rev. Lett.* **68** 674 (1992)
67. Kravchenko S V et al. *Phys. Rev. B* **42** 3741 (1990)
68. Efros A L *Solid State Commun.* **65** 1281 (1988)
69. Fano G, Ortolani F *Phys. Rev. B* **37** 8179 (1988)
70. Kukushkin I V, v. Klitzing K, Eberl K *Phys. Rev. Lett.* **82** 3665 (1999)
71. Usher A et al. *Phys. Rev. B* **41** 1129 (1990)
72. Bychkov Yu A, Iordanskii S V, Eliashberg G M *JETP Lett.* **33** 143 (1981); *Pis'ma Zh. Eksp. Teor. Fiz.* **33** 152 (1981)
73. Kallin C, Halperin B I *Phys. Rev. B* **30** 5655 (1984)
74. Khrapai V S et al. *Phys. Rev. B* **72** 035344 (2005)
75. Smith A P, MacDonald A H, Gumbs G *Phys. Rev. B* **45** 8829 (1992)
76. Sondhi S L et al. *Phys. Rev. B* **47** 16419 (1993)
77. Barrett S E et al. *Phys. Rev. Lett.* **74** 5112 (1995)
78. Khandelwal P et al. *Phys. Rev. Lett.* **86** 5353 (2001)
79. Brey L et al. *Phys. Rev. Lett.* **75** 2562 (1975)
80. Ashoori R C et al. *Phys. Rev. Lett.* **64** 681 (1990)
81. Ashoori R C et al. *Phys. Rev. B* **48** 4616 (1993)
82. Eisenstein J P, Pfeiffer L N, West K W *Phys. Rev. Lett.* **69** 3804 (1992)
83. Eisenstein J P, Pfeiffer L N, West K W *Phys. Rev. Lett.* **74** 1419 (1995)
84. Chan H B et al. *Phys. Rev. Lett.* **79** 2867 (1997)
85. Hatsugai Y, Bares P-A, Wen X G *Phys. Rev. Lett.* **71** 424 (1993)
86. He S, Platzman P M, Halperin B I *Phys. Rev. Lett.* **71** 777 (1993)
87. Levitov L S, Shytov A V *JETP Lett.* **66** 214 (1997); *Pis'ma Zh. Eksp. Teor. Fiz.* **66** 200 (1997)
88. Aleiner I L, Baranger H U, Glazman L I *Phys. Rev. Lett.* **74** 3435 (1995)
89. Dial O E et al. *Nature* **448** 176 (2007)
90. Dial O E et al. *Nature* **464** 566 (2010)
91. Dolgopolov V T et al. *Phys. Rev. B* **51** 7958 (1995)
92. Deviatov E V et al. *Phys. Rev. B* **61** 2939 (2000)
93. Yang S-R E, MacDonald A H *Phys. Rev. Lett.* **70** 4110 (1993)
94. Pikus F G, Efros A L *Phys. Rev. B* **51** 16871 (1995)
95. Lilly M P et al. *Phys. Rev. Lett.* **82** 394 (1999)
96. Koulakov A A, Fogler M M, Shklovskii B I *Phys. Rev. Lett.* **76** 499 (1996)
97. Fogler M M, Koulakov A A, Shklovskii B I *Phys. Rev. B* **54** 1853 (1996)
98. Fradkin E, Kivelson S A *Phys. Rev. B* **59** 8065 (1999)
99. Fradkin E et al. *Phys. Rev. Lett.* **84** 1982 (2000)
100. MacDonald A H, Fisher M P A *Phys. Rev. B* **61** 5724 (2000)
101. Wexler C, Dorsey A T *Phys. Rev. B* **64** 115312 (2001)
102. Pan W et al. *Phys. Rev. Lett.* **83** 820 (1999); cond-mat/9903160
103. Göres J et al. *Phys. Rev. Lett.* **99** 246402 (2007)
104. Cooper K B et al. *Phys. Rev. Lett.* **90** 226803 (2003)
105. Novoselov K S et al. *Science* **306** 666 (2004)
106. Novoselov K S et al. *Nature* **438** 197 (2005)
107. Geim A K, Novoselov K S *Nature Mater.* **6** 183 (2007)
108. Abanin D A et al. *Phys. Rev. Lett.* **98** 196806 (2007)
109. Novoselov K S et al. *Science* **315** 1379 (2007)
110. Entin M V et al., arXiv:1302.4829
111. Kozlov D A et al. *JETP Lett.* **93** 170 (2011); *Pis'ma Zh. Eksp. Teor. Fiz.* **93** 186 (2011)
112. Dolgopolov V T et al. *Phys. Rev. B* **59** 13235 (1999)
113. Raichev O E et al. *Phys. Rev. B* **86** 155320 (2012)
114. Gusev G M et al. *Phys. Rev. Lett.* **104** 166401 (2010)
115. Qi X-L, Zhang S-C *Rev. Mod. Phys.* **83** 1057 (2011)
116. König M et al. *Science* **318** 766 (2007)